J|A|C|S
ARTICLES
Published on Web 05/08/2002

Metallocene-Terminated Allylium Salts: The Effect of End Group on Localization in Polymethines

Stephen Barlow,*[,†,‡,§] Lawrence M. Henling,[†] Michael W. Day,[†] William P. Schaefer,[†] Jennifer C. Green,[‡] Tony Hascall,[‡] and Seth R. Marder[†,§,||]

Contribution from the Beckman Institute, 139-74, California Institute of Technology, Pasadena, California 91125, Inorganic Chemistry Laboratory, University of Oxford, South Parks Road, Oxford, OX1 3QR, U.K., Jet Propulsion Laboratory, California Institute of Technology, Pasadena, California 91109, and Department of Chemistry, University of Arizona, Tucson, Arizona 85721

Received November 5, 2001

Abstract: A range of 1,3-di(metallocenyl)allylium salts $[Mc(CH)_3Mc']^+[X]^-$ {Mc, Mc′ = ferrocenyl (Fc), 2,3,4,5,1′,2′,3′,4′-octamethylferrocen-1-yl (Fc″), ruthenocenyl (Rc); X = BF_4, PF_6} was synthesized by reaction of (2-lithiovinyl)metallocenes with formylmetallocenes, followed by treatment of the resulting alcohols with HX. Two salts with X = BAr′$_4$ {Ar′ = 3,5-$(CF_3)_2C_6H_3$} were synthesized by anion metathesis from the corresponding PF_6 salts. The crystal structure of $[Fc''(CH)_3Fc'']^+[PF_6]^-$ contains symmetrical termethine cations, while the same appears to be true in the disordered structure of $[Fc(CH)_3Fc]^+[PF_6]^-$. The formally unsymmetrical cation in $[Fc(CH)_3Fc']^+[BF_4]^-$ is only slightly unsymmetrical with little bond-length alternation in the allylium bridge. In contrast, the crystal structures of $[Rc(CH)_3Rc]^+[PF_6]^-$ and $[Rc(CH)_3Rc]^+[BAr'_4]^-$ both contain a bond-alternated "Peierls-distorted" cation, which can be considered as a ruthenocene bridged to a [(η^6-fulvene)(η^5-cyclopentadienyl)ruthenium] cation by a vinylene moiety. The strong similarity between solid-state and solution infrared and Raman spectra of $[BF_4]^-$, $[PF_6]^-$, and $[BAr'_4]^-$ salts of $[Rc(CH)_3Rc]^+$ indicates that the C−C stretching constant in the allylium chain and, therefore, the structure, of this ion are largely independent of the local environment, suggesting that the unsymmetrical structures observed in the crystal structures are not simply an artifact of packing. Differences in the solvatochromism of $[Rc(CH)_3Rc]^+$ and $[Fc(CH)_3Fc]^+$ also suggest a localized structure for the former cation in solution. Electrochemistry, UV−visible−NIR spectroscopy, and DF calculations give insight into the electronic structure of the metallocene-terminated allylium cations. Using an analogy between polymethines and mixed-valence compounds, the difference between the behaviors of $[Fc(CH)_3Fc]^+$ and $[Rc(CH)_3Rc]^+$ is attributed to larger reorganization energy associated with the geometry differences between metallocene and [(η^6-fulvene)(η^5-cyclopentadienyl)metal] structures in the ruthenium case.

Introduction

Typical polymethine cations or anions (cyanines) have C_{2v}-symmetric delocalized structures in which the C−C bond lengths are all approximately equal; the structure of a simple polymethine is well described as shown in Figure 1a; i.e., with equal contributions from two limiting resonance forms. However, it is predicted[1−3] that at sufficiently long chain lengths polymethines are subject to the Peierls distortion.[4] Where the end group can stabilize the overall charge, the structure of a Peierls-distorted polymethine is unsymmetrical with a polyene-like bond-length alternation (BLA) between formally single and double bonds; it is now dominated by *one* of the two extreme resonance forms (Figure 1b). Tolbert and Zhao reported the first experimental evidence for a localized polymethine; the com-

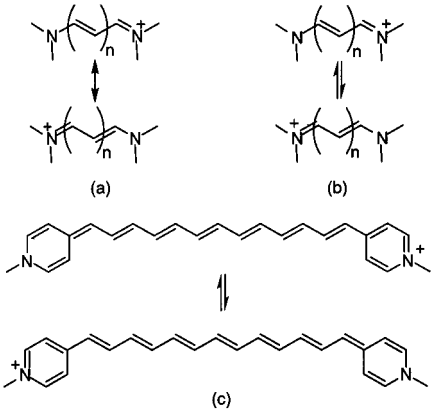

Figure 1. Representations of the structures of (a) a typical polymethine, (b) a Peierls-distorted polymethine, and (c) the Peierls-distorted polymethine reported by Tolbert and Zhao.[5]

* Author to whom correspondence should be addressed (University of Arizona). E-mail: sbarlow@email.arizona.edu.
† Beckman Institute, California Institute of Technology.
‡ University of Oxford.
§ University of Arizona.
|| Jet Propulsion Laboratory, California Institute of Technology.

(1) Kuhn, C. *Synth. Met.* **1991**, *41−43*, 3681−3688.
(2) Craw, J. S.; Reimers, J. R.; Bacskay, G. B.; Wong, A. T.; Hush, N. S. *Chem. Phys.* **1992**, *167*, 77−99.
(3) Tolbert, L. M.; Ogle, M. E. *Synth. Met.* **1992**, 391−396.
(4) Peierls, R. E. *Quantum Theory of Solids*; OUP: Oxford, 1955.

pound shown in Figure 1c was shown to be unsymmetrical by comparison of its IR and UV−visible−NIR spectra with those of symmetrical lower homologues.[5] The localization to an unsymmetrical structure can be understood by reference to mixed-valence chemistry;[5,6] symmetrical and Peierls-distorted polymethines are analogous to Robin and Day[7] class III and class II systems, respectively.

This paper is concerned with the effect of the end group on localization in polymethines. Work by Tolbert[3,8,9] has distinguished between organic polymethines where the end groups can stabilize the overall charge and those where they cannot. In the former case, the distortion localizes the charge on one end, as shown in Figure 1b. In the latter case, for example, in phenyl-terminated polymethine anions, the charge is centered in the middle of the chain, extending over approximately 15 carbon atoms in both directions. Similar differences in behavior between amino-terminated polyene/polymethine cations and phenyl-terminated polyene anions were predicted by Hush and co-workers.[2,10] We were interested in whether the choice of charge-stabilizing end group could affect the chain length at which localization occurred, as might be anticipated from the previously mentioned analogy with mixed-valence chemistry. The classification of a mixed-valence species in the class I/II/III spectrum is determined by the interplay of electronic coupling between the two alternative localized structures, V, and the vertical reorganization energy of Marcus theory, λ.[11,12] Thus, increased λ should cause a polymethine to localize at shorter chain length. One contribution to λ is the energy required to invert the sense of the BLA of the localized polymethine chain, λ_{bla}; another is the energy required to interconvert the geometries of the charged and uncharged (e.g., $H_2N^+ =$ vs H_2N-) forms of the end groups, λ_{end}. In the case of various organic donors or acceptors, and for many organometallic donors, this end group effect is limited to changing one or two bond lengths. The good conjugation between the end group and the polymethine chain leads to V sufficiently large to dominate until rather large chain length. The group 8 metallocenes might be expected to have somewhat different reorganization-energy characteristics. The resonance structure important in stabilizing carbocations α to metallocenes is considered to be the [(η^6-fulvene)(η^5-cyclopentadienyl)metal] cation (Figure 2a).[13] These structures differ significantly in geometry from the neutral metallocenes, the exo C−C bond being distorted from the plane of the fulvene to allow interaction of the α-carbon with the metal atom.[14−18] We were

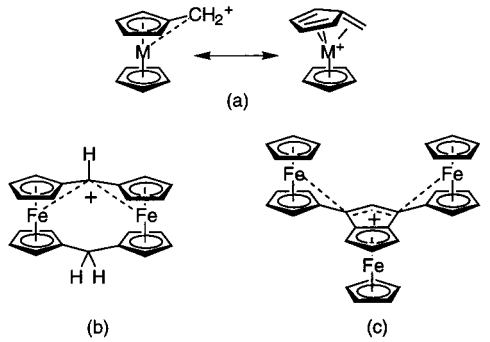

Figure 2. (a) Stabilization of a metallocenyl carbocation by resonance with a [(η^6-fulvene)(η^5-cyclopentadienyl)metal] cation, (b) a [1.1]metallocenophane carbocation, and (c) a crystallographically characterized trimetallic termethine reported by Schottenberger, Bildstein, and co-workers.[27]

Chart 1

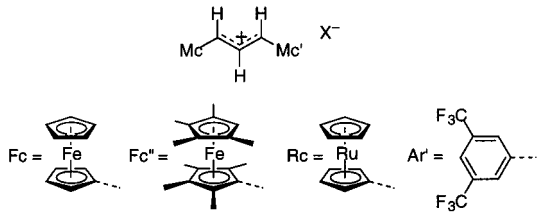

			salts isolated		
Mc	Mc'	cation	X = BF_4	PF_6	BAr'_4
Fc	Fc	1^+	**1a**	**1b**	**1c**
Fc"	Fc"	2^+	**2a**	**2b**	
Rc	Rc	3^+	**3a**	**3b**	**3c**
Fc	Fc"	4^+	**4a**		
Fc	Rc	5^+	**5a**	**5b**	

interested to see whether these large structural differences would lead to a large λ_{end}; moreover, differences between iron and ruthenium systems offered the possibility of tuning λ_{end}. Previous work on metallocene-terminated polymethines has been largely limited to ferrocene compounds, $[Fc(CH)_nFc]^+$. The $n = 1$ member, the bis(ferrocenyl)methylium ion, has been the subject of several studies,[19−22] including a crystal structure determination showing an essentially symmetrical cation in the tetrafluoroborate.[23] The cations formed by hydride abstraction from the bridges of [1.1]ferrocenophanes (Figure 2b)[24] can be regarded as derivatives of $[FcCHFc]^+$. The $[Fc(CH)_3Fc]^+$, $\mathbf{1}^+$, cation (Chart 1) has also been reported on several occasions,[22,25−27] and the closely related cation shown in Figure 2c has been shown to be essentially symmetrical in the crystal structure of its tetrafluoroborate.[27] Tolbert and co-workers synthesized a series of $[Fc(CH)_nFc]^+[BF_4]^-$ with $n = 1$, 3, 5, 9, 13 and reported electrochemical data and the low-energy UV−visible−NIR absorption maxima.[22] We recently reported that the [Rc-

(5) Tolbert, L. M.; Zhao, X. *J. Am. Chem. Soc.* **1997**, *119*, 3253−3258.
(6) Nelsen, S. F.; Tran, H. Q.; Nagy, M. A. *J. Am. Chem. Soc.* **1998**, *120*, 298−304.
(7) Robin, M. B.; Day, P. *Adv. Inorg. Chem. Radiochem.* **1967**, *10*, 247−422.
(8) Tolbert, L. M.; Ogle, M. E. *J. Am. Chem. Soc.* **1990**, *112*, 9519−9527.
(9) Tolbert, L. M. *Acc. Chem. Res.* **1992**, *25*, 561−568 and references therein.
(10) Craw, J. S.; Reimers, J. R.; Bacskay, G. B.; Wong, A. T.; Hush, N. S. *Chem. Phys.* **1992**, *167*, 101−109.
(11) Hush, N. S. *Chem. Phys.* **1975**, *10*, 361−362.
(12) It should also be noted that class II-type behavior is also favored by introduction of formal asymmetry into the system; i.e., by making the two extreme structures unequal in energy.
(13) Watts, W. E. In *Comprehensive Organometallic Chemistry*; Wilkinson, G., Stone, F. G. A., Abel, E. W., Eds.; Pergamon: London, 1988; Vol. 8.
(14) Behrens, U. *J. Organomet. Chem.* **1979**, *182*, 89−98.
(15) Yanovsky, A. I.; Struchkov, Y. T.; Kreindlin, A. Z.; Rybinskaya, M. I. *J. Organomet. Chem.* **1989**, *369*, 125−130.
(16) Rybinskaya, M. I.; Kreindlin, A. Z.; Struchkov, Y. T.; Yanovsky, A. I. *J. Organomet. Chem.* **1989**, *359*, 233−243.
(17) Kreindlin, A. Z.; Dolgushin, F. M.; Yanovsky, A. I.; Kerzina, Z. A.; Petrovskii, P. V.; Rybinskaya, M. I. *J. Organomet. Chem.* **2000**, *616*, 106−111.
(18) Barlow, S.; Cowley, A. R.; Green, J. C.; Brunker, T. J.; Hascall, T. *Organometallics* **2001**, *20*, 5351−5359.
(19) Boev, V. I.; Dombrovskii, A. V. *Zh. Obshch. Khim.* **1980**, *50*, 2520−2525.
(20) Jutz, C. *Tetrahedron Lett.* **1959**, 1−4.
(21) Bildstein, B.; Denifl, P.; Wurst, K. *J. Organomet. Chem.* **1995**, *496*, 175−186.
(22) Tolbert, L. M.; Zhao, X.; Ding, Y.; Bottomley, L. A. *J. Am. Chem. Soc.* **1995**, *117*, 12891−12892.
(23) Cais, M.; Dani, S.; Herbstein, F. H.; Kapon, M. *J. Am. Chem. Soc.* **1978**, *100*, 5554−5558.
(24) Mueller-Westerhoff, U. T.; Nazzal, A.; Prössdorf, W.; Meyerle, J. J.; Collins, R. L. *Angew. Chem., Int. Ed. Eng.* **1982**, *21*, 293−294.
(25) Bunton, C. A.; Carrasco, N.; Watts, W. E. *J. Chem. Soc., Perkin Trans. 2* **1979**, 1267−1273.
(26) Boev, V. I.; Dombrovskii, A. V. *Zh. Obshch. Khim.* **1985**, *55*, 1173−1177.
(27) Lukasser, J.; Angleitner, H.; Schottenberger, H.; Kopacka, H.; Schweiger, M.; Bildstein, B.; Ongania, K.-H.; Wurst, K. *Organometallics* **1995**, *14*, 5566−5578.

Scheme 1

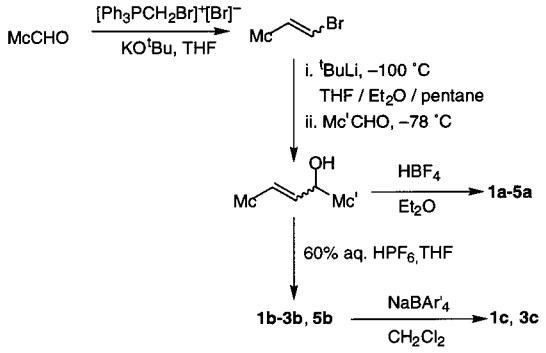

$(CH)_3Rc]^+$, $\mathbf{3}^+$, cation is markedly unsymmetrical in the crystal structure of its hexafluorophosphate, **3b**.[28] In this paper, we present evidence supporting an unsymmetrical structure for the $\mathbf{3}^+$ cation in other salts and in solution and report a comparative structural, electrochemical, and spectroscopic study of symmetrical and unsymmetrical allylium (termethine) cations with ferrocenyl (Fc), 2,3,4,5,1′,2′,3′,4′-octamethylferrocen-1-yl (Fc″) and ruthenocenyl (Rc) capping groups. The cations studied ($\mathbf{1}^+$−$\mathbf{5}^+$), and their salts (**1a**−**5a**, **1b**−**3b**, **5b**, **1c**, **3c**), are defined in Chart 1.

Results and Discussion

Synthesis. A range of metallocene-terminated allylium $[BF_4]^-$, $[PF_6]^-$, and $[BAr'_4]^-$ {Ar′ = 3,5-bis(trifluoromethyl)-phenyl} salts (see Chart 1) was synthesized as shown in Scheme 1. The known compound 1-ferrocenyl-2-bromoethene[29] and its new octamethylferrocenyl and ruthenocenyl analogues were readily obtained from the Wittig reaction between the corresponding aldehydes and bromomethyltriphenylphosphonium bromide,[30] some elimination to the alkyne[31,32] being observed in the ruthenium case. Bromine−lithium exchange, followed by reaction with metallocenyl aldehydes, afforded 1,3-dimetallocenylprop-1-ene-3-ols. (*E*)-FcCH═CHCH(OH)Fc was previously synthesized from (*E*)-FcCH═CHC(O)Fc;[25−27] since it has been found to be unstable with respect to reoxidation to the ketone,[27] and since pure products are obtained from the crude alcohols in the next step, we used our alcohols without full purification and characterization. Pure tetrafluoroborate and hexafluophosphate salts of the 1,3-di(metallocenyl)allylium cations were obtained after treatment with the appropriate acid, followed by crystallization from dichloromethane layered with diethyl ether.[33] Two $[BAr'_4]^-$ {Ar′ = 3,5-$(CF_3)_2C_6H_3$} salts, **1c** and **3c**, were synthesized using the metathesis reaction between the corresponding hexafluorophosphates and $[Na]^+[BAr'_4]^-$. The salts were studied by X-ray crystallography, cyclic voltammetry, and by electronic, vibrational, and NMR spectroscopy

Solid-State Structures. We have determined the crystal structures of **1b**, **2b**, **3b**, and **3c**, which contain symmetrically substituted allylium cations, as well as those of the formally unsymmetrical species **4a** and **5b**. Some important bond lengths and angles, defined in Figure 3, are compared in Table 1. Details of the structure determinations are given in Table 4, the Experimental Section, and the Supporting Information.

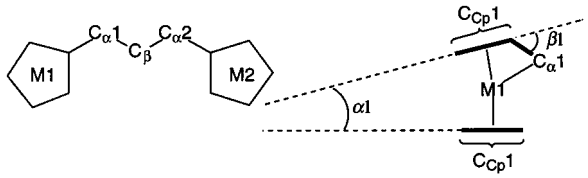

Figure 3. Schematic showing the definitions of some of the parameters given in Table 1 and used in discussing the crystal structures of the 1,3-di(metallocenyl)allylium cations.

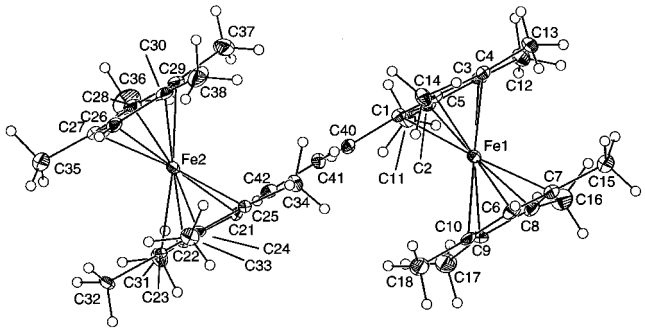

Figure 4. View of the $\mathbf{2}^+$ cation, $[Fc''(CH)_3Fc'']^+$, in the crystal structure of its hexafluorophosphate, **2b**. Non-hydrogen atoms are represented by 50% probability ellipsoids, while hydrogens are shown as spheres of arbitrary radius.

The apparent bond lengths in the allylium bridge of **1b** are affected by disorder. However, both ferrocenyl end groups appear to show comparable distortions from ideal ferrocene geometry; both the magnitude and slight asymmetry of these distortions are comparable with those found in the structures of $[FcCHFc]^+[BF_4]^-$[23] and of the tetrafluoroborate salt of the cation shown in Figure 2c.[27] In both of these previous structures, and in that of a [1.1]ferrocenophane-based cation[24] (Figure 2b) the C−C bond lengths indicate symmetrical bridging groups. Thus, it seems likely that **1b** is a typical, class III-like, polymethine. The $\mathbf{1}^+$ cation adopts a syn conformation in the crystal of **1b** (the cation shown in Figure 2c is also syn), with both iron atoms on the same face of the bridging ligand, giving the cation approximate C_s symmetry.

The structure of the $\mathbf{2}^+$ cation in **2b** (Figure 4) is clearly delocalized (class III-like); the bond lengths in the allylium bridge are not affected by disorder and clearly indicate an absence of BLA. The two octamethylferrocenyl groups show similar distortions, less extensive than those in the recently reported nonamethylferrocenylmethylium cation, where values of 2.567(12) Å and 23° were found for the Fe−C_α bond length and β, respectively, in the crystal structure of its $[BAr'_4]^-$ salt.[17] The distortions of the end groups are less marked than those in the structures of **1b** and of previously reported di(ferrocenyl) cations,[23,24,27] presumably reflecting the role played by the electron-donating methyl groups in stabilizing the allylium cation, reducing the need for donation from the metal. The $\mathbf{2}^+$ cation has approximate C_2 (rather than C_s) symmetry in the structure of **2b**; i.e., it adopts an anti conformation in which the two metallocene moieties are twisted away from one another (as might be expected from steric considerations); in all the other structures, the two metallocenes are syn.

(28) Barlow, S.; Henling, L. M.; Day, M. W.; Marder, S. R. *Chem. Commun.* **1999**, 1567−1568.
(29) FcCH═CHBr has also been obtained from the reaction of $FcCH{=}CHCO_2H$ and *N*-bromosuccinimide (Naskar, D.; Das, S. K.; Giribabu, L.; Maiya, B. G.; Roy, S. *Organometallics* **2000**, *19*, 1464−1469), and from the reaction of $FcCH{=}CHSnPh_3$ and bromine (Nesmeyanov, A.; Borisov, A. E.; Novikova, N. V. *Izv. Akad. Nauk. SSSR, Ser. Khim.* **1972**, 1372−1375).
(30) Driscoll, J. S.; Grisely, D. W.; Pustinger, J. V.; Harris, J. E.; Matthews, C. N. *J. Org. Chem.* **1964**, *29*, 2427−2431.
(31) Hofer, O.; Schlögl, K. *J. Organomet. Chem.* **1968**, *13*, 443−456.
(32) Rausch, M. D.; Siegel, A. *J. Org. Chem.* **1969**, *34*, 1974−1976.

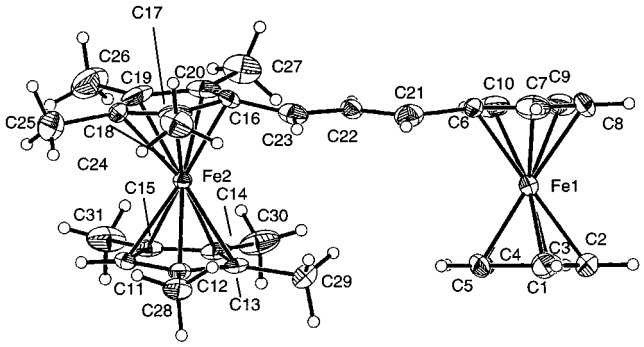

Figure 5. View of the $\mathbf{4}^+$ cation, $[Fc(CH)_3Fc'']^+$, in the crystal structure of its tetrafluoroborate, **4a**. Non-hydrogen atoms are represented by 50% probability ellipsoids, while hydrogens are shown as spheres of arbitrary radius.

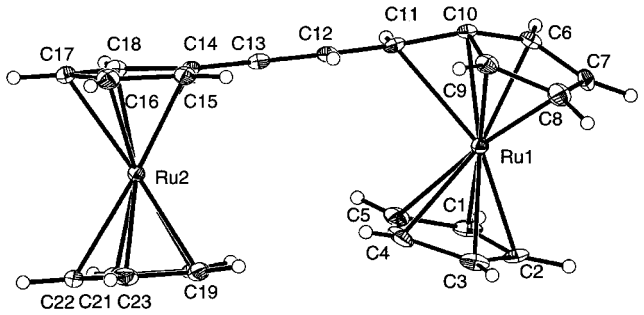

Figure 6. View of the $\mathbf{3}^+$ cation, $[Rc(CH)_3Rc]^+$, in the crystal structure of its hexafluorophosphate, **3b**. Non-hydrogen atoms are represented by 50% probability ellipsoids, while hydrogens are shown as spheres of arbitrary radius.

The unsymmetrical species **4a** also adopts a delocalized structure (Figure 5); the BLA of 0.023(9) Å is insignificant at the 3σ level. However, the data do show the octamethylferrocene moiety to be more distorted than the ferrocene, reflecting a greater contribution to stabilization of the charge from its higher lying HOMO. Thus, the $\mathbf{4}^+$ cation seems best described as a hybrid of the $Fc''^+{=}CH{-}CH{=}CH{-}Fc$ and $Fc''{-}CH{=}CH{-}CH{=}Fc^+$ resonance structures, but with the former structure being somewhat more important due to its lower energy. The appropriate mixed-valence analogy is an inherently unsymmetrical class III species (the appropriate potential well diagram is shown in Figure 4c of ref 34).

The remaining structures are localized. **3b** (Figure 6) is the first crystallographically characterized Peierls-distorted polymethine.[35,36] One of the two ruthenocenes (that containing Ru1) is best described as a [(η^6-fulvene)(η^5-cyclopentadienyl)ruthenium]$^+$ moiety; the values of M1$-$C$_\alpha$1, α_1, and β_1 in Table 1 are similar to the corresponding values of previously reported ruthenocenyl carbocation structures (ranges 2.270(3)$-$2.571(4) Å, 29.1$-$42.6°, and 7.1$-$12.9°, respectively,[15,18,37−39] excluding values for the severely disordered structure of [Cp*Ru(η^6-C$_5$Me$_4$CH$_2$)]$^+$[PF$_6$]$^-$ [40]) and with parameters obtained in a DFT optimization of $[RcCH_2]^+$ (2.025$-$2.254 Å, 2.263 Å, 5.3°, and 41.2° for Ru$-$C$_{Cp}$, Ru$-$C$_\alpha$, α, and β, respectively).[18,41] In contrast, the Ru2 ruthenocene has "normal" ruthenocene geometry; the Ru$-$C$_{Cp}$ distances fall in ranges similar to those for ruthenocene itself (2.181(2)$-$2.188(2) Å)[42] and for its derivatives such as (*E*)-1,2-dimethyl-1,2-diruthenocenylethene (2.171(3)$-$2.216(3) Å).[43] The α-carbon, C13, is very slightly bent *away* from Ru2 with a very long and, therefore, nonbonded Ru$-$C$_\alpha$ distance. The allylium bridge shows significant BLA; the formally double and single CH$-$CH bonds differ in length by 0.100(6) Å. The structure can, therefore, be described as ruthenocene and [(η^6-fulvene)(η^5-cyclopentadienyl)ruthenium]$^+$ moieties linked by an vinylene bridge.

The structure of **5b** is isomorphous with that of **3b**; the $\mathbf{5}^+$ cation is composed of a "normal" ferrocene with a vinylene bridge to a [(η^6-fulvene)(η^5-cyclopentadienyl)ruthenium] unit. Thus, ruthenocene is clearly more effective than ferrocene in stabilizing the positive charge in these systems, in accord with what is known about the stability of simple metallocenyl carbocations,[44] with electrochemical and spectroscopic data (vide infra) and with the previously reported structures of [FcCHRc]$^+$[PF$_6$]$^-$[37] and of salts of a mixed iron$-$ruthenium [1.1]metallocenophane cationic derivative.[37,38] The main differences from the structure of **3b**, apart from the expected differences in the metal$-$carbon bond lengths in the "normal" metallocene unit, are in the disorder of the hexafluorophosphate counterions. The bond lengths in the allylium bridge of **5b** are identical, within experimental error, to the corresponding values for **3b**, as is the Ru1$-$C$_\alpha$ bond length.

An important question that arises is whether the unsymmetrical structure of the cation in **3b** arises from the influence of crystal-packing effects. The [(η^6-fulvene)(η^5-cyclopentadienyl)ruthenium]$^+$ moiety of **3b** is approached more closely by hexafluorophosphate anions than the "normal" ruthenocene. Is this due to the effect of the unsymmetrical cation on the crystal packing, or does this packing determine the cation symmetry? Evidence for the former hypothesis is provided by comparison of the packing diagrams for **1b** and **3b**, which are quite similar (Figure 7). Moreover, such severe effects of counterion upon polymethines have not previously been reported,[36] although effects of counterion and packing motif upon the intramolecular electron-transfer rate in class II mixed-valence compounds are

(33) Attempts to synthesize the tetrafluoroborate of the mixed octamethylferrocenyl/ruthenocenyl species led to a mixture of $[Fc''(CH)_3Rc]^+[BF_4]^-$ and $[Fc''(CH)_3Rc]^{2+}([BF_4]^-)_2$, as shown by elemental analysis and by a crystal structure determination for the dicationic species (Barlow, S.; Day, M. W.; Marder, S. R. *Acta Crystallogr.* **2000**, *C56*, 303−304). The electrochemical data for the reaction product do indeed indicate a more easily oxidized iron center than any of the other species studied.

(34) Creutz, C. *Prog. Inorg. Chem.* **1983**, *30*, 1−73.

(35) Dähne and Reck have reported a more subtle asymmetry (bond-length alternation of ~0.01 Å) in the crystal structure of $[Me_2N(CH)_7NMe_2]^+[BPh_4]^-$ (Dähne, L.; Reck, G. *Angew. Chem., Int. Ed. Engl.* **1995**, *34*, 690−692). An even more subtle asymmetry is reported in the structure of the corresponding picrate salt (Dähne, L.; Reck, G. *Z. Kristallogr.* **1995**, *210*, 948−951). This effect is absent with inorganic counterions, even when, as in the $[BF_4]^-$ salt (Dähne, L.; Grahn, W.; Jones, P. G.; Chrapkowski, A. *Z. Kristallogr.* **1994**, *209*, 54−516), they are unsymmetrically arranged relative to the cations and has, therefore, been attributed to polarization of the polymethine π-system by interactions with the aromatic rings of the anion.

(36) Although one crystal structure of an organic cyanine has been claimed as evidence for unsymmetrical localization (Borowiak, T. E.; Bokii, N. G.; Struchkov, Y. T. *Zh. Strukt. Khim.* **1972**, *13*, 480), Smith has pointed out that the apparent bond-length alternation is insignificant, given the large standard deviations for the relevant interatomic distances (Smith, D. L. *Photogr. Sci. Eng.* **1974**, *18*, 309−322).

(37) Watanabe, M.; Motoyama, I.; Takayama, T. *Bull. Chem. Soc. Jpn.* **1996**, *69*, 2877−2884.

(38) Watanabe, M.; Moyoyama, I.; Takayama, T. *J. Organomet. Chem* **1996**, *524*, 9−18.

(39) Sato, M.; Kawata, Y.; Kudo, A.; Iwai, A.; Saitoh, H.; Ochiai, S. *J. Chem. Soc., Dalton Trans.* **1998**, 2215−2224.

(40) Kreindlin, A. Z.; Petrovskii, P. V.; Rybinskaya, M. I.; Yanovskii, A. I.; Struchkov, Y. T. *J. Organomet. Chem.* **1987**, *319*, 229−237.

(41) A similar geometry was found in a MNDO/AM1 study: Gal'pern, E. G.; Gambaryan, N. P.; Kreindlin, A. Z.; Rybinskaya, M. I.; Stankevich, I. V.; Chistyakov, A. L. *Metalloorg. Khim.* **1992**, *5*, 831−838.

(42) Seiler, P.; Dunitz, J. D. *Acta Crystallogr.* **1980**, *B36*, 2946−2950.

(43) Chiu, C.-F.; Song, M.; Chen, B.-H.; Kwan, K. S. *Inorg. Chim. Acta* **1997**, *266*, 73−79.

(44) Hill, E. A.; Richards, J. H. *J. Am. Chem. Soc.* **1961**, *83*, 3840−3846.

Table 1. Selected Crystallographically Determined Geometric Parameters (Defined in Figure 3) for 1,3-Di(metallocenyl)allylium Salts

	1b (M1 = Fe1, M2 = Fe2)	**2b** (M1 = Fe1, M2 = Fe2)	**3b** (M1 = Ru1, M2 = Ru2)	**3c** (M1 = Ru1, M2 = Ru2)	**4a** (M1 = Fe1 {Fc}, M2 = Fe2 {Fc″})	**5b** (M1 = Ru, M2 = Fe)
M1−$C_{Cp}1^a$/Å	2.001(6)−2.064(6)	2.032(3)−2.079(3)	2.089(2)−2.234(3)	2.100(7)−2.221(7)	2.010(5)−2.057(5)	2.080(3)−2.217(4)
M2−$C_{Cp}2^a$/Å	2.009(6)−2.058(7)	2.048(3)−2.076(3)	2.167(2)−2.194(3)	2.139(7)−2.199(7)	2.028(4)−2.093(4)	2.038(4)−2.065(4)
M1−$C_\alpha1^b$/Å	2.834(7)	3.024(3)	2.381(3)	2.604(8)	3.017(4)	2.385(4)
M2−$C_\alpha2^b$/Å	2.933(7)	3.031(3)	3.237(3)	3.104(8)	2.837(4)	3.151(4)
$C_\alpha1-C_\beta{}^c$/Å	1.469(10)[f]	1.379(4)	1.443(4)	1.452(10)	1.380(6)	1.444(5)
$C_\alpha2-C_\beta{}^c$/Å	1.461(10)[f]	1.380(4)	1.343(4)	1.372(10)	1.403(6)	1.344(5)
$\alpha_1{}^d$/deg	4.8(4)	3.8(2)	9.0(2)	6.6(7)	1.4(2)	9.1(2)
$\alpha_2{}^d$/deg	13.4(4)	6.2(2)	4.0(2)	1.8(7)	8.2(2)	4.2(3)
$\beta_1{}^e$/deg	13.2	4.5	38.2	28.2	5.0	37.9
$\beta_2{}^e$/deg	9.1	4.7	−1.0	4.5	14.5	−0.4

[a] Range of bond lengths within the metallocene. [b] Distance from metal atom to the allylium carbon α to the metallocene. [c] Bond length from the allylium carbon α to the metallocene to the β-carbon (the central atom of the bridge). [d] Ring tilt; angle between the planes of the five-membered rings of the metallocene. [e] Angle between the $C_{ipso}-C_\alpha$ bond and the plane of the five-membered ring to which the α-carbon is bound. [f] Values severely affected by unmodeled disorder (see Experimental Section).

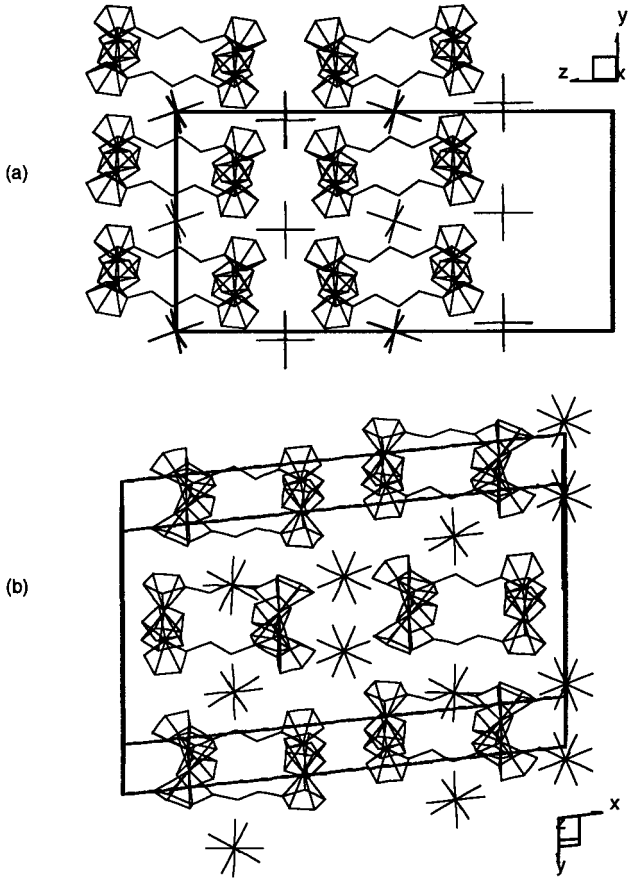

Figure 7. Packing diagrams for (a) **1b** and (b) **3b**.

well known. Nevertheless, we further investigated the influence of the counterion by crystallizing the $\mathbf{3}^+$ cation with the weaklycoordinating, delocalized $[BAr'_4]^-$ {Ar′ = 3,5-$(CF_3)_2C_6H_3$} anion. The structure of the $\mathbf{3}^+$ cation in **3c** (Figure 8) is similar to that in **3b**. First, there is a clear BLA of 0.080(14) Å in the allylium bridge (indistinguishable at the 3σ level from that in **3b**). Second, only one of the end groups shows distortion toward the η^6-fulvene structure; although this distortion is a little less severe than that in **3b**, with somewhat longer Ru−C_α distance and a smaller β, these parameters are very close to the range for previously reported ruthenocenyl carbocation structures and β and Ru−C_α have previously been shown to vary with crystal packing in salts of $[RcCH_2]^+$[18] and of a mixed iron−ruthenium [1.1]metallocenophane cation.[37,38] The localized structure of the

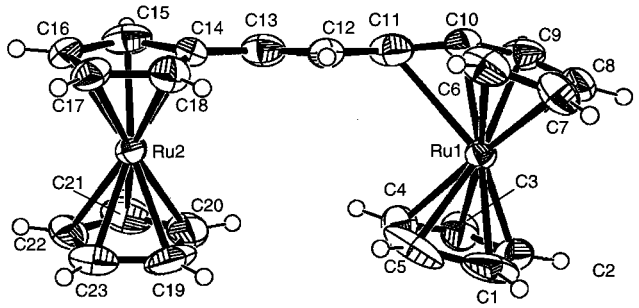

Figure 8. View of the $\mathbf{3}^+$ cation, $[Rc(CH)_3Rc]^+$, in the crystal structure of its $[BAr'_4]^-$ salt, **3c**. Non-hydrogen atoms are represented by 50% probability ellipsoids, while hydrogens are shown as spheres of arbitrary radius.

$\mathbf{3}^+$ cation in both **3b** and **3c** suggests that the localization is not significantly dependent upon the nature of the counterions.

UV−Visible−NIR Spectroscopy and Orbital Structure. UV−visible−NIR spectra were recorded for the 1,3-di(metallocenyl)allylium salts in a variety of solvents, the use of the $[BAr'_4]^-$ ion enabling spectra of the $\mathbf{1}^+$ and $\mathbf{3}^+$ cations to be acquired in some solvents of low polarity. For a given cation, essentially identical spectra were obtained for $[BF_4]^-$, $[PF_6]^-$, and $[BAr'_4]^-$ salts. Our data for $\mathbf{1}^+$ salts were similar to the published data.[27]

The UV−visible−NIR spectra of the metallocene-terminated allylium cations (Figure 9) resemble the spectra of metallocene−(π-bridge)−acceptor second-order nonlinear optical (NLO) dyes;[45] both classes of compounds show two prominent absorptions, hereafter referred to as the low-energy (LE) and high-energy (HE) absorptions. The orbital structures obtained for $\mathbf{1}^+$ and $\mathbf{3}^+$ cations using DF calculations based upon the crystallographically determined geometries (details of which are given in the Experimental Section) support this analogy. As in the NLO dyes,[46] the highest occupied orbitals are metal d-based orbitals, below which is an orbital (π) composed of an out-of-phase combination of the HOMOs of the cyclopentadienyl and π-bridge fragments (π is the HOMO-6 for a symmetrical structure, where the filled d-orbitals of both metallocenes are higher in energy, and the HOMO-3 for unsymmetrical cations, where the three highest occupied orbitals are all localized on the "normal" metallocene). The LUMO has π* character.

(45) Barlow, S.; Marder, S. R. *Chem. Commun.* **2000**, 1555−1562.
(46) Barlow, S.; Bunting, H. E.; Ringham, C.; Green, J. C.; Bublitz, G. U.; Boxer, S. G.; Perry, J. W.; Marder, S. R. *J. Am. Chem. Soc.* **1999**, *121*, 3715−3723.

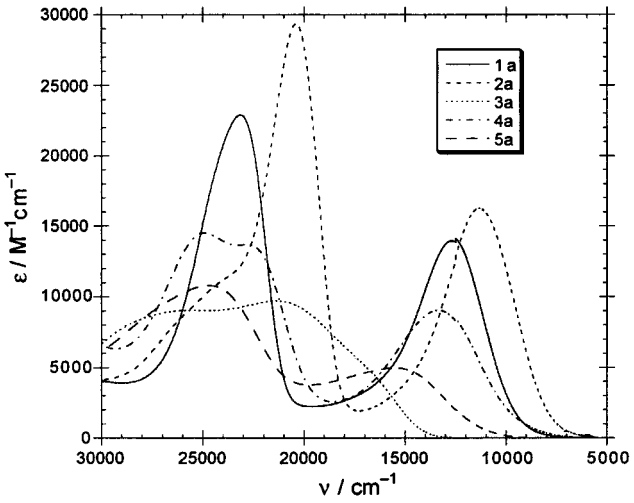

Figure 9. UV-visible−NIR spectra of bis(metallocenyl)allylium cations in dichloromethane.

Isosurfaces for π and π^* of the two ions are shown in Figure 10; these are clearly similar to the HOMO-3 and LUMO of the NLO dyes (Figure 5 of ref 46). In the case of the unsymmetrical cation, the LUMO is more localized toward the formally cationic end of the molecule, and the highest π orbital is localized toward the "normal" metallocene end. Nonetheless, Figure 10 shows that the important orbitals do not change very dramatically in form or extent on breaking the symmetry. In analogy with the assignment of the spectra of the NLO dyes,[46] and consistent with our orbital scheme, we assign the LE band of the metallocene allylium species to a metal-to-π^* transition and the HE band to a π-to-π^* transition.

The assignment is further supported by the differences in the spectra of different metallocene polymethines. Comparing the two absorption maxima of $[FcCHFc]^+$,[19] $\mathbf{1}^+$, and $[Fc(CH)_5Fc]^+$[47] cations shows the energy of the HE band to be more sensitive to chain length,[45] consistent with our assignment, which predicts that the energy of the HE band will depend on the energies of both π (which will be raised by increasing chain length) and π^* (which will be lowered), while the LE band should depend on the energies of metal-based d-orbitals (more-or-less unchanged with chain length) and on π^*. Moreover, the variation of the energy of the HE band with effective conjugation length closely parallels that for the $[Ph(CH)_nPh]^+$ series, as shown in Figure 7 of ref 45. In $\mathbf{2}^+$, methylation should raise both the filled metal d-orbitals and the highest filled π orbital, consistent with the observed red shifts of both bands. Replacement of Fe by Ru leads to blue shifts of 0.35 and 1.07 eV for the HE and LE bands, respectively. A metal-to-π^* band should be more sensitive to metal identity than a π-to-π^* band, consistent with our assignment (ruthenocene has a lower energy HOMO than ferrocene[48]). The shift in the HE band partly reflects some metal contribution to π and π^* but will also be affected if, as proposed, $\mathbf{3}^+$ has an unsymmetrical structure.

Since the intervalence charge-transfer spectra of class II and class III mixed-valence compounds show different patterns of solvatochromism,[34] similar differences are anticipated between some absorptions of localized and delocalized polymethines.

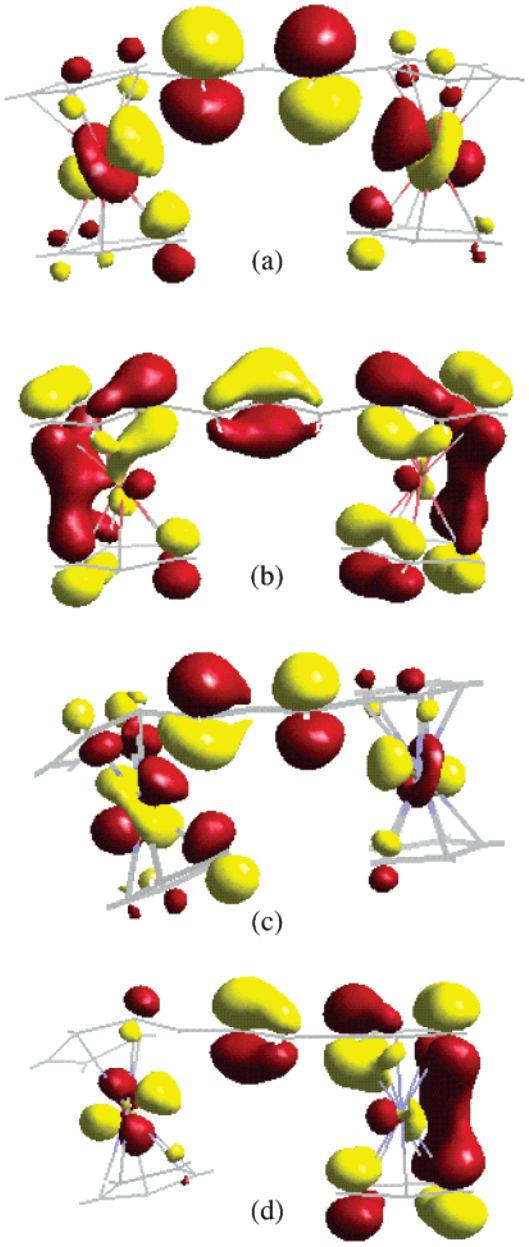

Figure 10. DF molecular orbitals for the $\mathbf{1}^+$—(a) the π^* LUMO and (b) the highest lying π orbital—and $\mathbf{3}^+$ cations—(c) π^* and (d) π.

Indeed the π-to-π^* transition of the compound shown in Figure 1c showed a much stronger variation of $\bar{\nu}_{max}$ with $1/n^2 - 1/D$, where n and D are the solvent refractive index and dielectric constant, respectively, than those of shorter homologues.[5] The solvent dependence indicates a decrease or a reversal in dipole moment between ground and excited state; this is due to the greater charge-transfer character of the transition due to localization of the π HOMO toward the quinoidal end of the molecule and of the π^* LUMO toward the formally cationic end as shown in Figure 8 of ref 5 (in this respect, the Peierls-distorted polymethine resembles a donor−acceptor polyene). Similarly, our calculations show that the donor orbitals—both metal-based and π-based—and the π^* acceptor orbital of an unsymmetrical di(metallocenyl)allylium cation are more localized toward "normal" and formally cationic ends, respectively, than in a symmetrical species and, therefore, that both the metal-to-π^* and π-to-π^* transitions should have more charge-transfer

(47) Barlow, S.; Perrins, L. Unpublished results.
(48) Cauletti, C.; Green, J. C.; Kelly, M. R.; Robbins, J.; Smart, J. C. *J. Electron Spectrosc. Relat. Phenom.* **1980**, *19*, 327−353.

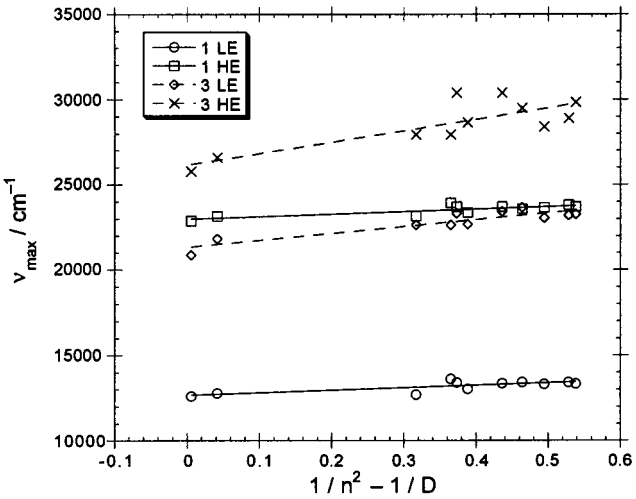

Figure 11. Solvatochromism of the $\mathbf{1}^+$ and $\mathbf{3}^+$ cations. The scatter in the data for the high-energy band of the **3** cation reflects the difficulty of accurately determining the peak position, due to overlap with the low-energy band. The solvents used were, in order of increasing $1/n^2 - 1/D$: benzene, 1,4-dioxane, Et_2O, EtOAc, THF, PhCN, DMSO, DMF, acetone, MeCN, and MeOH.

character. The solvent dependence of the spectra of $\mathbf{3}^+$ was, therefore, compared with that of $\mathbf{1}^+$. Figure 11 compares the variation of both LE and HE maxima for $\mathbf{1}^+$ and $\mathbf{3}^+$ with the polarity of a range of nonhalogenated solvents.[49] The stronger dependence of $\bar{\nu}_{max}$ with $1/n^2 - 1/D$ clearly supports an unsymmetrical solution structure for $\mathbf{3}^+$. In addition, it can be seen from Figure 9 that the absorption bands for $\mathbf{3}^+$ and $\mathbf{5}^+$ are somewhat broader than those for $\mathbf{1}^+$, $\mathbf{2}^+$, and $\mathbf{4}^+$, also consistent with class II-like behavior for the first two cations; the unsymmetrical cation in Figure 1c was also reported to show a broader π-to-π^* transition than its lower symmetrical homologues.[5]

IR Spectroscopy. Infrared spectroscopy of salts of the 1,3-di(metallocenyl)allylium salts reveals a strong band in the range ~1550−1600 cm^{-1} (Table 2), which we assign to a stretching mode of the multiply bonded allylium bridge (neither ruthenocene, the counterions used, nor the [(η^6-fulvene)(η^5-cyclopentadienyl)ruthenium] cation[18] shows a band in this region). Despite complications arising from absorption of the laser fundamental, we were also able to observe this band in the Raman spectra of a number of compounds (see Experimental Section). Calculations by Reimers and Hush predict that symmetrical and unsymmetrical (Peierls-distorted) forms of $[NH_2(CH)_nNH_2]^+$ (n = 19, 25) have different vibrational frequencies.[50] The insensitivity of the allylium band of the $\mathbf{3}^+$ cation to counterion and to medium suggests that its structure

Table 2. Selected IR Data for 1,3-Di(metallocenyl)allylium Salts in the Solid State and in Dichloromethane Solution

	$\bar{\nu}_{allylium}$/cm^{-1}	
compd	KBr	CH_2Cl_2
1a	1548	1560
1b	1558	1558
1c	1561	1555
2a	1548	1538
2b	1538	1542
3a	1603	1601
3b	1609	1598
3c	1584	1600
4a	1553	1556
5a	1598	1596
5b	1598	1599

in solution and in its crystalline $[BF_4]^-$ salt is the same as it is in crystals of its $[PF_6]^-$ and $[BAr'_4]^-$ salts (where the cation is known to be unsymmetrical by X-ray crystallography, vide supra). Moreover, $\mathbf{3}^+$ salts show bands (1584−1603 cm^{-1}) at similar frequency to those of the $\mathbf{5}^+$ cation (1596−1599 cm^{-1}), which is markedly unsymmetrical in both the crystal structure of its hexafluorophosphate and in solution (according to ^{1}H NMR spectroscopy, vide infra). The symmetrical $\mathbf{1}^+$ (1548−1560 cm^{-1}) and $\mathbf{2}^+$ (1538−1561 cm^{-1}) cations show allylium bands significantly lower in frequency than the $\mathbf{3}^+$ and $\mathbf{5}^+$ cations. The formally unsymmetrical $\mathbf{4}^+$ cation (1553−6 cm^{-1}) shows a band at similar frequency to the delocalized $\mathbf{1}^+$ and $\mathbf{2}^+$ cations. This is consistent with both crystallographic and NMR data, both of which show considerably less BLA in the allylium bridge of the $\mathbf{4}^+$ cation than in that of the $\mathbf{5}^+$ cation.

NMR Spectroscopy. The three nominally symmetrical allylium cations, $\mathbf{1}^+$, $\mathbf{2}^+$, and $\mathbf{3}^+$, all show room-temperature ^{1}H and ^{13}C NMR spectra consistent with symmetrical structures. The observation of a symmetrical solution structure for $\mathbf{3}^+$ is not particularly surprising since the cation is likely to be fluxional on the NMR time scale (which is, of course, much longer than the time scales for electronic and vibrational spectroscopies); the Peierls-distorted polymethine (Figure 1c) previously reported by Tolbert and Zhao is also symmetrical on the NMR time scale.[5] We attempted to "freeze out" the interconversion between the two alternative unsymmetrical structures of $\mathbf{3}^+$ by recording spectra for **3a** in dichloromethane-d_2 solution at temperatures down to −85 °C (500 MHz for ^{1}H and 125 MHz for ^{13}C). Although some chemical shifts changed considerably and some of the resonances corresponding to the ruthenocenyl moieties were very considerably broadened in both ^{1}H and ^{13}C spectra, there was relatively little broadening of bridge ^{1}H and ^{13}C resonances and the ^{1}H−^{1}H coupling constant associated with the allylium bridge was unchanged. This suggests that the process being affected is not the interconversion of the two extreme structures; an alternative possibility is that we are observing slowing of rotation of the ruthenocenyl end groups about the Rc−C$_\alpha$ bonds. The failure to observe localization by NMR allows the rate of interconversion between the two extreme structures to be estimated as in excess of 4000 s^{-1} down to −85 °C, corresponding to a barrier of less than 32.3 kJ mol^{-1} (≡ 0.33 eV ≡ 2700 cm^{-1}).[51]

The mixed ferrocenyl/ruthenocenyl species, $\mathbf{5}^+$, appears to have an unsymmetrical bridge according to ^{1}H−^{1}H coupling constants (12.2, 14.5 Hz), consistent with the BLA seen in the crystal structure of **5b** (vide supra). In the octamethylferrocenyl/

(49) If halogenated solvents are included, considerably more scatter is introduced to the plots for both $\mathbf{1}^+$ and $\mathbf{3}^+$ cations, although the best-fit lines are still steeper for the diruthenium species. In particular, absorption maxima for all our metallocenyl allylium cations are considerably more red-shifted in dichloromethane than might be expected from simple solvent polarity or polarizability parameters. Similar behavior has been observed for charge-transfer-type bands in other metallocene systems (for example, see data and graph in the Supporting Information for ref 46, and Figure 4 in: Barlow, S. *Inorg. Chem.* **2001**, *40*, 7047−7053) and may indicate some sort of specific interaction between metallocenes and chlorinated solvents. Indeed, it has been found that ν_{max} for the intervalence charge-transfer transitions of $[FcN{=}NFc]^+$ do not correlate well with $1/n^2 - 1/D$ for chlorinated solvents but that better correlation is found if ν_{max} is plotted against $150-(1/n^2 - 1/D) - (AN - DN)$, where AN and DN are the solvent acceptor and donor numbers, respectively: Kurosawa, M.; Nankawa, T.; Matsuda, T.; Kubo, K.; Kurihara, M.; Nishihara, H. *Inorg. Chem.* **1999**, *38*, 5113−5123.

(50) Reimers, J. R.; Hush, N. S. *Chem. Phys.* **1993**, *176*, 407−420.

Table 3. Electrochemical Half-Wave Potentials (mV, vs Ferrocenium/Ferrocene) for Symmetrical and Unsymmetrical 1,3-Di(metallocenyl)allylium Cations in THF and Dichloromethane ($\sim 10^{-4}$ M **1a**−**5a**, 0.1 M $[Bu_4N]^+[PF_6]^-$, 50 mV s^{-1})

	THF			CH_2Cl_2		
cation, C^+	C^+/C^a	C^{2+}/C^{+b}	C^{3+}/C^{2+c}	C^+/C^a	C^{2+}/C^{+b}	C^{3+}/C^{2+c}
$\mathbf{1}^+$	−670	+145	+645	−635	+210	+820
$\mathbf{2}^+$	−930	−140	+385	−965	−120	+580
$\mathbf{3}^+$	−715	$E_{ox} = \sim +455^d$		−760	$E_{ox} = \sim +570^d$	
$\mathbf{4}^+$	−785	−55	+500	−805	−10	+740
$\mathbf{5}^+$	−705	+70	$E_{ox} = \sim +455^d$	−730	+115	$E_{ox} = \sim +540^d$

[a−c] $^+$/C, C^{2+}/C^+, and C^{3+}/C^{2+} are half-wave potentials vs ferrocenium/ferrocene for the $[Mc(CH)_3Mc']^+/[Mc(CH)_3Mc']^\bullet$, $[Mc(CH)_3Mc']^{2+}/[Mc(CH)_3Mc']^+$, and $[Mc(CH)_3Mc']^{3+}/[Mc(CH)_3Mc']^{2+}$ couples, respectively. [d] Irreversible; potential of oxidation peak given.

ferrocenyl species, $\mathbf{4}^+$, there is less variation in the bridge $^1H-^1H$ coupling constants (13.1, 14.2 Hz), consistent with the reduced BLA seen in the structure of **4a** and with the infrared data.

The ^{13}C shift of C_β, the central C of the allylium bridge, δ_β, is related to the π-charge density, ρ_β, at that atom by $\rho_\beta = (\delta_\beta - \delta_o)/c$,[8,52] where δ_o and c are constants (the relationship between δ_α and ρ_α will be less straightforward due to the effects of direct interaction with the metal). Comparison of the NMR data for $\mathbf{1}^+$ ($\delta_\beta = 125.3$ ppm) and $\mathbf{3}^+$ ($\delta_\beta = 119.6$ ppm) cations clearly shows less positive charge density in the diruthenium compound, indicating greater stabilization of the positive charge by ruthenocene end groups, consistent with electrochemical data (vide infra). Moreover, the shift for $\mathbf{5}^+$ (120.8 ppm) indicates that most of the extra stabilization effected by ruthenocene can be effected by just one ruthenocene, also consistent with electrochemical data (vide infra) and with a localized structure for the $\mathbf{3}^+$ cation.

Electrochemistry. Cyclic voltammetric data for the bis(metallocenyl)allylium tetrafluoroborates (**1a**−**5a**) are summarized in Table 3.[53] For each of the diiron cations, $\mathbf{1}^+$, $\mathbf{2}^+$, and $\mathbf{4}^+$, three one-electron redox processes were observed (voltammograms for $\mathbf{2}^+$ are shown in the Supporting Information). The C^{2+}/C^+ couple was observed at positive potential relative to oxidation of the parent metallocene[54] and showed reversibility comparable to that of ferrocenium/ferrocene under the same conditions. Processes at higher and lower potentials are attributed to C^{3+}/C^{2+} and C^+/C couples, respectively; both show characteristic features of EC processes (i.e., those where the electron transfer itself is reversible but where the oxidized species undergoes a chemical reaction on a time scale comparable with that of the electron transfer) and cycling to potentials approaching those for these couples leads to the buildup of features we attribute to decomposition products.[55] The ruthenocene portions of $\mathbf{3}^+$ and $\mathbf{5}^+$ undergo irreversible oxidation, as does ruthenocene itself,[56] while the C^+/C features in these compounds resembled those of the diiron cations. The C^+/C data allow comparison of the abilities of the various metallocenes to stabilize positive charge.[57] The diruthenocene cation $\mathbf{3}^+$ is 45 mV (in THF) harder to reduce than its diferrocene analogue $\mathbf{1}^+$, indicating greater stabilization of the positive charge in the former case. There is only a small difference (10 mV in THF) in the ease of reduction of $\mathbf{3}^+$ and $\mathbf{5}^+$, suggesting that only one ruthenocene can effect most of the charge stabilization, consistent with a localized structure for $\mathbf{3}^+$. The octamethylferrocene compounds are harder still to reduce, presumably largely due to the inductive effect of the methyl groups.

Summary

We have synthesized and characterized a range of 1,3-di(metallocenyl)allylium cations. The metallocenes stabilize the carbocationic charge through contributions from [(η^6-fulvene)-(η^5-cyclopentadienyl)metal] cation structures. The $[Fc(CH)_3Fc]^+$, $\mathbf{1}^+$, and $[Fc''(CH)_3Fc'']^+$, $\mathbf{2}^+$, cations are symmetrical species. The terminal ferrocenes are less distorted toward a [(η^6-fulvene)-(η^5-cyclopentadienyl)iron] structure in $\mathbf{2}^+$ due to the stabilizing effect of the methyl groups upon the positive charge. The formally unsymmetrical $[Fc(CH)_3Fc'']^+$, $\mathbf{4}^+$, cation is electronically somewhat unsymmetrical according to crystallographic and NMR data. However, this asymmetry is insufficient to result in crystallographically significant BLA in the allylium bridge. The vibrational spectrum shows a C−C stretch attributable to the allylium bridge at a frequency similar to the symmetrical $\mathbf{1}^+$ and $\mathbf{2}^+$ cations. This cation can, therefore, be regarded delocalized, despite its inherent asymmetry.

Replacement of ferrocenyl with ruthenocenyl leads to rather different properties. The crystal structures of $[Rc(CH)_3Rc]^+[PF_6]^-$,

(51) The rate and the barrier were estimated as follows. We assumed the ^{13}C frequency of the C_5H_5 of the cationic end of the localized molecule (ν_1) will be approximately the same as that of the $\mathbf{5}^+$ cation, while the frequency of the other C_5H_5 group (ν_2) can be estimated by assuming that the value observed for the $\mathbf{3}^+$ cation (ν_{obs}) is an average of ν_1 and ν_2. The rate constant, k, obeys the inequality, $k > \pi(\nu_1 - \nu_2)/\sqrt{2}$, while the barrier height, $\Delta G^\ddagger$, is related to k by, $k = (k_B T/h) \exp(-\Delta G^\ddagger/RT)$. Similar results are obtained by assuming ν_1 and ν_2 to be equal to the C_5H_5 ^{13}C frequencies of the ruthenocenylmethylium cation (ref 18) and ruthenocene, respectively.

(52) Spiesecke, H.; Schneider, W. G. *Tetrahedron Lett.* **1961**, 468−72.

(53) It has previously been reported that the polymethines $[Fc(CH)_nFc]^+[BF_4]^-$ (n = 1, 3, 5, 9, 13) undergo two oxidations in dichloromethane (ref 22); the values reported for **1a** correspond to potentials of −40 and +140 mV vs ferrocenium/ferrocene, clearly at variance with our values. We suggest that it is possible that the previous measurements may have been complicated by the presence of the decomposition products (see ref 55) of $\mathbf{1}^+$, which we observed at $E_{1/2} = \sim +10$ mV in dichloromethane.

(54) 1,2,3,4,1′,2′,3′,4-Octamethylferrocene is oxidized at −360 and −445 mV vs ferrocenium/ferrocene in THF and CH_2Cl_2, respectively: Mendiratta, A.; Barlow, S.; Day, M. W.; Marder, S. R. *Organometallics* **1999**, *18*, 454−456.

(55) When potentials approaching C^{3+}/C^{2+} were employed, an additional feature was found to grow in at a potential similar to the parent metallocene, its intensity increasing with successive cycles. Similar features are seen when the potential is cycled around C^+/C; these features are presumably due to the products of the side reactions associated with C^{3+}/C^{2+} and C^+/C. In the case of $\mathbf{1}^+$ in THF, at least some of the decomposed material was found to be adhering to the working electrode. When the electrodes were removed from the analyte solution, rinsed with fresh solvent, and inserted into fresh THF electrolyte solution, a feature was observed with peak potentials $E_{ox} = +20$ mV and $E_{red} = -20$ mV ($E_{ox} = +5$ mV and $E_{red} = -15$ mV in CH_2Cl_2). It was previously shown that reduction of $[FcCHFc]^+$ to the radical is followed by dimerization (Tirouflet, J.; Laviron, E.; Moise, C.; Mugnier, Y. *J. Organomet. Chem.* **1973**, *50*, 241−6) so some of the new signals observed may be due to dimerized species.

(56) Diaz, A. F.; Mueller-Westerhoff, U. T.; Nazzar, A.; Tanner, M. *J. Organomet. Chem.* **1982**, *236*, C45−C48 and references therein.

(57) All the 1,3-di(metallocenyl)allylium cations are considerably more readily reduced than the ruthenocenylmethylium cation, presumably due to more delocalized lower-energy π^*-type LUMOs in the present compounds; the LUMO of the monomeric species is much more localized on ruthenium (ref 18).

3b, $[Rc(CH)_3Rc]^+[BAr'_4]^-$, **3c**, and $[Fc(CH)_3Rc]^+[PF_6]^-$, **5b**, are all markedly unsymmetrical and comprise a [(η^6-fulvene)-(η^5-cyclopentadienyl)ruthenium] cation linked by a vinylene bridge to an undistorted metallocene. The structures of **3b** and **3c** are the first of Peierls-distorted polymethines; i.e., symmetrically substituted species that adopt an unsymmetrical structure with polyene-like bond-length alternation and in which the overall charge is localized on only one of the two end groups. Localization in **3c**, despite the noncoordinating delocalized counterion, suggests the asymmetry is due to an inherent property of the cation rather than to crystal-packing effects. Fast time-scale spectroscopic techniques are also consistent with an instantaneously unsymmetrical structure for $\mathbf{3}^+$ in solution; the allylium C−C stretching frequencies are similar for $\mathbf{3}^+$ and $\mathbf{5}^+$ cations and significantly different from those for $\mathbf{1}^+$, $\mathbf{2}^+$, and $\mathbf{4}^+$, and, moreover, the frequencies for $\mathbf{3}^+$ salts are similar in solution and in the solid. The electronic spectrum of $\mathbf{3}^+$ shows broader absorptions, more strongly dependent upon solvent polarity, than that of $\mathbf{1}^+$, also consistent with a localized solution structure for $\mathbf{3}^+$. On the (slower) NMR time scale, a symmetrized structure is observed for $\mathbf{3}^+$.

The behavior of $\mathbf{3}^+$ parallels that of many class II mixed-valence compounds where the apparent delocalization depends on the time scale of the technique used and often varies between solution and the solid state. The difference in behavior between $\mathbf{1}^+$ and $\mathbf{3}^+$ cations can also be rationalized using an analogy with mixed-valence chemistry; localization in the diruthenium compound may be due to a larger reorganization energy in the metallocene/[(η^6-fulvene)(η^5-cyclopentadienyl)metal] system for ruthenium than for iron, presumably connected with the greater tendency toward η^6 coordination found for the larger metal. Control of the reorganization energy in this way may be a useful design principle for the synthesis of other charge-localized polymethines. Furthermore, tuning the reorganization energy could be used as a method of controlling the barrier height between the two extreme localized forms of the molecule. In principle, the sense of the bond-length alternation could be reversed by application of an external electric field, leading to a large change in polarization, which could be exploited in optical and electronic applications.

Experimental Details

General Considerations. Elemental analyses were performed by Atlantic Microlab Inc. (Norcross, GA) or by the Inorganic Chemistry Laboratory's Analytical Service. Most NMR spectra were recorded using a General Electric QE-300 spectrometer. Variable-temperature data were acquired using a Varian Unity Plus 500 spectrometer; data are reported for room temperature (~25 °C), unless stated otherwise. UV−visible−NIR spectra were acquired using Hewlett-Packard 8452A spectrometers, a Varian Cary 5E spectrometer, or a GBC Instruments Cintra 10 spectrometer. IR spectra were acquired with a Perkin-Elmer Spectrum 1000 spectrometer; Raman spectra were acquired with a Nicolet Raman 950 instrument, using the 633-nm line of a He/Ne laser at a power of 1 mW. Solid samples were run as either neat powders or mixed with KBr. Cyclic voltammetry was performed under argon on dry tetrahydrofuran or dichloromethane solutions ~10^{-4} M in sample and 0.1 M in $[^nBu_4N]^+[PF_6]^-$ using a glassy carbon working electrode, a platinum auxiliary electrode, a AgCl/Ag pseudoreference electrode, and a BAS 100B potentiostat. Potentials were referenced by the addition of ferrocene to the cell and are quoted relative to the nearest 5 mV relative to the ferrocenium/ferrocene couple at 0 V. Where necessary, solvents were distilled from calcium hydride (dichloromethane) or sodium benzophenone ketyl (THF, diethyl ether, pentane).

Computational Methods. Single-point calculations were carried out using the Amsterdam Density Functional package (ADF99).[58] The electronic configurations were described by an uncontracted triple-ζ basis set of Slater orbitals, with a single polarization functional added to the main group atoms. The cores were frozen up to 2p for Fe, 3p for Ru, and 1s for C. Relativistic corrections were included using the ZORA formalism. The structures of the cations were taken from those in the crystal structures of **1b** and **3b**, the bond lengths in the bridge of $\mathbf{1}^+$ being modified from the apparent values from the disordered crystal to chemically reasonable values ($C_{Cp}-C_\alpha$, 1.43 Å; $C_\alpha-C_\beta$, 1.38 Å, as in the structure of **2b**). C−H bond distances were set at 1.09 Å. Energies were calculated using Vosko, Wilk, and Nusair's local exchange correction,[59] with nonlocal exchange corrections by Becke,[60] and nonlocal exchange correlation corrections by Perdew.[61,62]

General Procedure for 1-Metallocenyl-2-bromoethenes, McCH═CHBr. A slurry of KO^{t}Bu (12.5 mmol) in dry THF (100 mL) was added dropwise under nitrogen to a slurry of $[Ph_3PCH_2Br]^+[Br]^-$ [30] (12.5 mol) in dry THF (100 mL) at −78 °C. After 1 h, a solution of the appropriate aldehyde (10 mmol) in dry THF (30 mL) was added dropwise. The reaction mixture was allowed to warm to room temperature and stirred at room temperature until the reaction was complete by TLC. Water and diethyl ether (100 mL each) were added, and the layers were separated. The aqueous layer was extracted with more ether (2 × 100 mL); the combined ether extracts were washed with saturated aqueous sodium chloride (2 × 100 mL), dried over magnesium sulfate, filtered, and evaporated under reduced pressure. Purification procedures are given below. The reactions were also carried out on scales of between 3 and 26 mmol.

FcCH═CHBr. The general procedure above was used to synthesize FcCH═CHBr[29] (6.33 g, 21.8 mmol, 84%) from FcCHO (5.56 g, 26.0 mmol); the reaction time was 13 h, and the crude product was purified by dissolving in hexane and passing through a silica plug. FcCH═CHBr (~1:2 *E*/*Z* isomer mixture) was obtained as an orange-red oil, crystallizing after prolonged drying in vacuo: ^{1}H NMR (300 MHz, benzene-d_6) (*E*-isomer) δ 6.66 (d, J = 14.0 Hz, 1H), 6.02 (d, J = 14.0 Hz), 3.92 (s, 5H), 3.87 (apparent s, 4H); ^{1}H NMR (300 MHz, benzene-d_6) (*Z*-isomer) δ 6.34 (d, J = 7.7 Hz, 1H), 5.85 (d, J = 7.7 Hz, 1H), 4.61 (t, J = 1.7 Hz, 2H), 4.03 (t, J = 1.7 Hz, 2H), 3.96 (s, 5H); ^{13}C NMR (75 MHz, benzene-d_6) (isomeric mixture) δ 135.2, 131.3, 102.8, 101.5, 81.9, 79.2, 70.1, 69.6, 69.5, 69.3, 69.2, 66.7; high-resolution EIMS calcd for $C_{12}H_{11}FeBr$ M^+ 289.9394, found 289.9396.

Fc″CH═CHBr. The general procedure above was used to synthesize Fc″CH═CHBr (2.53 g, 6.28 mmol, 57%) from Fc″CHO[63] (3.60 g, 11.0 mmol); the reaction time was 72 h and the crude product was purified by dissolving in hexane and passing through a silica plug. Fc″CH═CHBr (~2:3 *E*/*Z* isomer mixture) was obtained as an orange-red oil: ^{1}H NMR (300 MHz, benzene-d_6) (*E*-isomer) δ 6.96 (d, J = 14.0 Hz, 1H), 6.18 (d, J = 14.0 Hz, 1H), 3.10 (s, 1H), 1.66 (s, 6H), 1.62 (s, 6H), 1.56 (s, 6H), 1.52 (s, 6H); ^{1}H NMR (300 MHz, benzene-d_6) (*Z*-isomer) δ 6.78 (d, J = 7.4 Hz, 1H), 6.21 (d, J = 7.4 Hz, 1H), 3.15 (s, 1H), 1.65 (s, 6H), 1.60 (s, 6H), 1.59 (s, 6H), 1.56 (s, 6H); ^{13}C NMR (75 MHz, benzene-d_6) (isomeric mixture) δ 135.8, 131.9, 109.8, 101.0, 81.7, 80.9, 80.8, 80.7, 80.5, 80.1, 79.7, 79.0, 78.9, 77.4, 72.1, 72.0, 11.9, 11.5, 11.2, 10.2, 10.1, 9.6 (some methyl resonances presumably

(58) Baerends, E. J.; Berces, A.; Bo, C.; Boerringter, P. M.; Cavallo, L.; Deng, L.; Dickson, R. M.; Ellis, D. E.; Fan, L.; Fischer, T. H.; Fonseca Guerra, C.; van Gisbergen, S. J.; Groeneveld, J. A.; Gritsenko, O. V.; Harris, F. E.; van den Hoek, P.; Jacobsen, H.; van Kessel, G.; Kootstra, F.; van Lenthe, E.; Osinga, V. P.; Philipsen, P. H. T.; Post, D.; Pye, C. C.; Ravenek, W.; Ros, P.; Schipper, P. R. T.; Schreckenbach, G.; Snijiders, J. G.; Sola, M.; Swerhone, D.; te Velde, G.; Vernooijis, P.; Versluis, L.; Visser, O.; van Wezenbeek, E.; Wiesenekker, G.; Wolff, S. K.; Woo, T. K.; Ziegler, T. *ADF Program System Release 1999*; Department of Theoretical Chemistry, Vrije Universiteit: Amsterdam, 1999.
(59) Vosko, S. H.; Wilk, L.; Nusair, M. *Can. J. Phys.* **1990**, *58*, 1200.
(60) Becke, A. D. *Phys. Rev.* **1988**, *A38*, 3098−3100.
(61) Perdew, J. P. *Phys. Rev.* **1986**, *B34*, 7406.
(62) Perdew, J. P. *Phys. Rev.* **1986**, *B34*, 8822−8824.
(63) Zou, C.; Wrighton, M. S. *J. Am. Chem. Soc.* **1990**, *112*, 7578−7584.

coincident); high-resolution LSIMS calcd for $C_{20}H_{27}FeBr$ M^+ 402.0645, found 402.0647.

RcCH═CHBr and RcC≡CH. The general procedure above was used to synthesize RcCH═CHBr (700 mg, 2.09 mmol, 55%) from RcCHO[64] (984 mg, 3.80 mmol); the reaction time was 90 h, and the crude product was purified by flash chromatography on silica, eluting with hexane. Evaporation of the first fraction afforded RcCH═CHBr (~1:1 *E*/*Z* isomer mixture) as a yellowish oil, solidifying after prolonged drying in vacuo: ^{1}H NMR (300 MHz, benzene-d_6) (isomeric mixture) δ 6.59 (d, J = 13.8 Hz, 1H), 6.30 (d, J = 7.8 Hz, 1H), 6.00 (d, J = 13.8 Hz, 1H), 5.71 (d, J = 7.8 Hz, 1H), 5.04 (m, 2H), 4.44 (m, 2H), 4.39 (s, 5H), 4.38 (m, 2H), 4.33 (m, 2H), 4.31 (s, 5H); ^{13}C NMR (75 MHz, benzene-d_6) (isomeric mixture) δ 134.3, 130.4, 102.8, 102.1, 85.9, 83.2, 72.2, 71.6, 71.5, 71.2, 71.0, 69.0; high-resolution LSIMS calcd for $C_{12}H_{11}RuBr$ M^+ 337.9067, found 337.9078; Evaporation of the second fraction gave an off-white solid found to be RcC≡CH[31,32] (220 mg, 0.98 mmol, 26%): ^{1}H NMR (300 MHz, benzene-d_6) δ 4.82 (m, 2H), 4.42 (s, 5H), 4.26 (m, 2H), 2.41 (s, 1H); ^{13}C NMR (75 MHz, benzene-d_6) δ 81.8, 74.5, 74.4, 72.3, 71.1, 68.4; high-resolution LSIMS calcd for $C_{12}H_{10}Ru$ M^+ 255.9826, found 255.9823; IR (KBr) 3265 (vs), 3115, 3095, 2100 (s), 1439, 1404, 1260, 1220, 1096, 1027 (s), 9992, 902, 813 (s), 654 (s), 614, 555, 520 cm^{-1}.

General Procedure for Synthesis of 1,3-Dimetallocenylprop-1-ene-3-ols, McCH═CHCH(OH)Mc′. A 1-metallocenyl-2-bromoethene (2 mmol) was dissolved in a 1:1:4 mixture of pentane, diethyl ether, and THF (15 mL). The solution was cooled to −98 °C (MeOH/liquid N_2) and treated with a 1.7 M pentane solution of ^{t}BuLi (4 mmol). After 30 min, the reaction was allowed to warm to −78 °C over 30 min. The reaction mixture was then treated with a solution of the appropriate metallocenyl aldehyde (2 mmol) in THF (10 mL). After 15 min at −78 °C, the reaction mixture was allowed to warm to room temperature over 1 h and treated with water (20 mL) and diethyl ether (20 mL). The layers were separated, and the aqueous layer was extracted with three additional portions of ether. The combined ether extracts were dried over potassium carbonate, filtered, and evaporated under reduced pressure. Since the instability of FcCH═CHCH(OH)Fc with respect to oxidation to FcCH═CHC(O)Fc has previously been noted,[27] and since our octamethylferrocenyl alcohols appear even more unstable, we did not attempt to fully purify and characterize the alcohols. The crude materials were isolated as described below and used without purification in the synthesis of the allylium salts.

FcCH═CHCH(OH)Fc.[25−27] Crude FcCH═CHCH(OH)Fc[26,27] (912 mg, 2.14 mmol, 46%) was prepared from FcCH═CHBr (1.36 g, 4.68 mmol) andFcCHO (1.00 g, 4.67 mmol) by the general method and obtained as an orange powder in an ~1:2 *E*:*Z* isomer ratio, after recrystallization of the evaporation residue from hot heptane. Its identity was checked using NMR and mass spectroscopy before conversion to salts of **1**$^+$: ^{1}H NMR (300 MHz, benzene-d_6) (isomeric mixture) δ 6.39 (d, J = 15.7 Hz, 1H), 6.19 (d, J = 11.3 Hz, 2H), 6.12 (dd, J = 15.7, 6.3 Hz, 1H), 5.80 (dd, J = 10.9, 8.9 Hz, 2H), 5.49 (br, dd, 2H), 4.89 (br, apparent t, 1H), 4.91−3.91 (m), 1.79 (br d, 2H), 1.70 (br d, 1H); ^{13}C NMR (300 MHz, benzene-d_6) δ 131.5, 130.0, 93.3, 93.1, 83.3, 81.4, 71.9, 71.0−66.1 (numerous overlapping peaks but δ 69.5 and 68.8 are very strong), 61.7; LSIMS m/z 426 (57%, M^+), 409 (100%, M^+ − OH); high-resolution LSIMS calcd for $C_{23}H_{22}OFe_2$ M^+ 426.0369, found 426.0378.

RcCH═CHCH(OH)Rc. Crude RcCH═CHCH(OH)Rc (~1:1 isomer mixture) was obtained in a manner similar to its diiron analogue (off-white powder, 604 mg, 1.05 mmol 50%) from RcCH═CHBr (700 mg, 2.08 mmol) and RcCHO (540 mg, 2.08 mmol): ^{1}H NMR (300 MHz, benzene-d_6) (isomeric mixture) δ 6.38 (d, J = 15.6 Hz, 1H), 6.17 (d, J = 10.0 Hz, 1H), 6.00 (dd, J = 15.6, 6.2 Hz, 1H), 5.57−5.48 (overlapping dd and m, 3H), 4.84 (m, 2H), 4.77 (m, 2H), 4.73 (m, 3H), 4.71 (m. 1H), 4.66 (m, 2H), 4.59 (m, 1H), 4.49 (s, 5H), 4.48 (s, 5H), 4.44 (m, 2H), 4.42 (s, 5H), 4.41 (s, 5H), 4.37 (2 overlapping m, 3H), 1.58 (d, J = 6.8 Hz, 1H), 1.51 (d, J = 5.2 Hz, 1H); LSIMS *m*/*z* 518 (8%, M^+), 501 (10%, M^+ − OH); high-resolution LSIMS calcd for $C_{23}H_{22}ORu_2$ M^+ 517.9758, found 517.9760.

FcCH═CHCH(OH)Rc. Crude FcCH═CHCH(OH)Rc (~1:2 *E*:*Z* mixture) was obtained as a dull orange powder (419 mg, 0.89 mmol, 58%) from FcCH═CHBr (440 mg, 1.52 mmol) and RcCHO (393 mg, 1.52 mmol) in a fashion similar to the previous two compounds: ^{1}H NMR (300 MHz, benzene-d_6) (isomeric mixture) δ 6.45 (d, J = 15.7 Hz, 1H), 6.20 (d, J = 11.3 Hz, 2H), 6.05 (dd, J = 15.7, 6.2 Hz, 1H), 5.66 (dd, J = 11.3, 8.5, 2H), 5.43 (t, J = ~7.5 Hz, 2H), 4.75−3.90 (many overlapping peaks), 1.85 (d, J = 8.0 Hz), 1.62 (d, J = 7.0 Hz, 2H); high-resolution LSIMS calcd for $C_{23}H_{22}OFeRu$ M^+ 472.0064, found 472.0077.

Fc″CH═CHCH(OH)Fc″. This compound was synthesized by the general method from Fc″CH═CHBr (990 mg, 2.46 mmol) and Fc″CHO (800 mg, 2.45 mmol); it was obtained in crude form as a brown oil (1.36 g, 2.09 mmol, 85%), which decomposed on standing, after flash chromatography under nitrogen on basic alumina, eluting with ethyl acetate/hexanes (1:7). The desired fractions were identified by testing for a darkening (allylium cation formation) with concentrated HCl. Due to its instability, this compound was used directly without further purification or characterization.

FcCH═CHCH(OH)Fc″. Crude FcCH═CHCH(OH)Fc″ was obtained as a brown oil (0.96 g, 1.48 mmol, 41%) from FcCH═CHBr (1.06 g, 3.66 mmol) and Fc″CHO (1.19 g, 3.65 mmol) in analogy to the previous compound.

General Procedure for Tetrafluoroborate Salts of Metallocene-Terminated Allylium Cations. HBF_4 (1−2 mL, 85% solution in diethyl ether) was freeze−pump−thaw degassed and added dropwise to a deoxygenated solution of the appropriate alcohol precursor (100−200 mg) in a minimum quantity of dry diethyl ether (25−120 mL). The mixture instantly darkened and precipitation occurred. The supernatant was decanted by cannula, and the precipitate was washed with diethyl ether (2 × 25 mL) before drying in vacuo. The salts were crystallized by extraction into dichloromethane (~20 mL), filtration, and layering with diethyl ether (~200 mL).

General Procedure for Hexafluorophosphate Salts of Metallocene-Terminated Allylium Cations. Deoxygenated 60% aqueous hexafluorophosphoric acid (1 mL) was added dropwise to a stirred deoxygenated solution of the appropriate alcohol (0.5 mmol) in THF; the mixture instantly darkened. After 15 min, deoxygenated water (75 mL) was added, affording a dark precipitate. The precipitate was allowed to settle, and the supernatant was removed by cannula. The solids were washed with water (2 × 75 mL) and dried in vacuo, before extraction into dichloromethane (~20 mL), filtration, and crystallization by layering with diethyl ether (~200 mL).

[Fc(CH)$_3$Fc]$^+$[BF$_4$]$^-$[27] (1a). Pure **1a** (80 mg, 0.16 mmol, 70%) was obtained by the general procedure from the corresponding crude alcohol (100 mg, 0.23 mmol): ^{1}H NMR (300 MHz, dichloromethane-d_2) δ 8.39 (d, J = 13.4 Hz, 2H), 6.49 (t, J = 13.4 Hz, 1H), 5.59 (apparent s, 4H), 5.05 (apparent s, 4H), 4.51 (s, 10H); ^{13}C NMR (75 MHz, dichloromethane-d_2) δ 157.3, 125.3, 87.5, 83.5, 76.3, 74.0; high-resolution LSIMS calcd for $C_{23}H_{21}Fe_2$ M^+ − BF_4 409.0342, found 409.0342; UV (CH_2Cl_2) λ_{max} 431 (ϵ_{431} 23 000), 787 (ϵ_{787} 14000) nm; UV ($CHCl_3$) λ_{max} 428, 772 nm; UV (THF) λ_{max} 422, 746 nm; UV (EtOAc) λ_{max} 418, 734 nm; UV (MeCN) λ_{max} 420, 745 nm; UV (MeOH) λ_{max} 422, 750 nm; UV (DMSO) λ_{max} 422, 748 nm; UV (DMF) λ_{max} 424, 744 nm; UV (acetone) λ_{max} 423, 751 nm; UV (PhCN) λ_{max} 428, 766 nm; UV (H_2O) λ_{max} 414, 730 nm; IR (KBr) 3095, 1548 (s), 1444, 1414, 1374, 1280, 1225, 1156, 1066 (s, br), 917, 833, 634 cm^{-1}; IR (CH_2Cl_2) 1560, 1093, 1025, 835 cm^{-1}. Anal. Calcd for $C_{23}H_{21}BF_4Fe_2$: C, 55.71; H, 4.27. Found: C, 55.61; H, 4.30.

[Fc(CH)$_3$Fc]$^+$[PF$_6$]$^-$ (1b). Red crystals of pure **1b** (170 mg, 0.31 mmol, 58%) were obtained from the corresponding crude alcohol (225

(64) Sanders, R.; Mueller-Westerhoff, U. T. *J. Organomet. Chem.* **1996**, *512*, 219−224.

mg, 0.53 mmol) using the general method: IR (KBr) 3115, 1558 (vs), 1449 (s), 1409, 1374, 1284, 1225 (s), 1161, 1106, 1056, 982, 828 (vs), 634, 555 cm^{-1}; IR (CH_2Cl_2) 1558 (s), 1450, 1225, 846 (s) cm^{-1}; Raman (CH_2Cl_2) 1542 cm^{-1}. Anal. Calcd for $C_{23}H_{21}PF_6Fe_2$: C, 49.85; H, 3.82. Found: C, 49.66; H, 3.82.

[Fc(CH)$_3$Fc]$^+$[BAr′$_4$]$^-$ {Ar′ = 3,5-Bis(trifluoromethyl)phenyl} (1c). Pure **1c** (120 mg, 0.094 mmol, 76%) was obtained from **1b** (120 mg, 0.14 mmol) and [Na]$^+$[BAr′$_4$]$^-$[65] (110 mg, 0.12 mmol) using the method described by Manríquez and co-workers for the synthesis of [FeCp$_2$]$^+$[BAr′$_4$]$^-$:[66] UV (Et_2O) λ_{max} 432, 787 nm; UV (1,4-dioxane) λ_{max} 432, 782 nm; UV (benzene) λ_{max} 437, 793 nm; IR (KBr) 1561 (vs), 1453, 1357 (s), 1278 (vs), 1235, 1128 (vs, br), 890, 840, 832, 713, 683, 669. 642 cm^{-1}; IR (CH_2Cl_2) 1558 (s), 1451, 1355 (s), 1284 (vs), 1229, 1127 (vs, br), 897 (s), 839, 672, 635 cm^{-1}. Anal. Calcd for $C_{55}H_{33}BF_{24}Fe_2$: C, 51.92; H, 2.61. Found: C, 51.74; H, 3.31.

[Fc″(CH)$_3$Fc″]$^+$[BF$_4$]$^-$ (2a). Dark green microcrystals of pure **2a** (180 mg, 0.25 mmol, 58%) were obtained from the corresponding crude alcohol (282 mg, 0.43 mmol) using the general method: ^{1}H NMR (300 MHz, dichloromethane-d_2) δ 8.08 (d, J = 13.7 Hz, 2H), 6.85 (t, J = 13.7 Hz, 1H), 3.58 (s, 1H), 1.99 (s, 12H), 1.80 (s, 12H), 1.50 (s, 12H), 1.46 (s, 12H); ^{13}C NMR (75 MHz, dichloromethane-d_2) δ 153.4, 127.1, 97.9, 88.1, 87.6, 86.3, 85.6, 76.3, 11.2, 11.0, 10.7, 9.2; high-resolution LSIMS calcd for $C_{39}H_{53}Fe_2$ M$^+$ − BF_4 633.2846, found 633.2868; UV (dichloromethane) λ_{max} 492 (ϵ_{492} 30 000), 880 (ϵ_{880} 16 000) nm; UV (THF) λ_{max} 477, 847 nm; UV (EtOAc) λ_{max} 478, 830 nm; UV (MeCN) λ_{max} 484, 850 nm; UV (DMSO) λ_{max} 480, 847 nm; IR (KBr) 2956, 2896, 2856, 1548 (s), 1478, 1450, 1404, 1379, 1240, 1175, 1056 (s, br), 1026 (s, br), 897, 674, 629, 609, 530 cm^{-1}; IR (CH_2Cl_2); 2951, 2910, 2868, 1538 (s), 1383, 1179, 1088 (s), 1025 (s) cm^{-1}; Anal. Calcd for $C_{39}H_{53}BF_4Fe_2$: C, 65.03; H, 7.43. Found: C, 64.78; H, 7.43.

[Fc″(CH)$_3$Fc″]$^+$[PF$_6$]$^-$ (2b). Green needles of pure **2b** (260 mg, 0.33 mmol, 58%) were obtained from the corresponding crude alcohol (375 mg, 0.58 mmol) using the general method. IR (KBr) 2946, 2916, 2856, 1538 (s), 1483, 1449, 1399, 1379, 1240, 1175, 1021, 840 (s), 634, 555 cm^{-1}; IR (CH_2Cl_2) 2951, 2910, 2868, 1542 (s), 1382, 1236, 1180, 1020, 846 (s); Anal. Calcd for $C_{39}H_{53}PF_6Fe_2$: C, 60.17; H, 6.86; Found: C, 60.40; H, 6.49.

[Rc(CH)$_3$Rc]$^+$[BF$_4$]$^-$ (3a). Pure **3a** (180 mg, 0.31, 46%) was obtained from the corresponding crude alcohol (345 mg, 0.67 mmol) using the general method: ^{1}H NMR (300 MHz, dichloromethane-d_2, 25 °C) δ 7.35 (d, J = 13.5 Hz, 2H), 6.17 (t, J = 13.5 Hz, 1H), 5.43 (t, J = 1.9 Hz, 4H), 5.18 (t, J = 1.9 Hz, 4H), 4.83 (s, 10H); ^{1}H NMR (500 MHz, dichloromethane-d_2, −85 °C) δ 7.06 (d, J = 13.3 Hz, 2H), 6.02 (t, J = 13.3 Hz, 1H), 5.33 (s, br, 4H), 5.08 (s, very br, 4H), 4.72 (apparently two overlapping s, 10H); ^{13}C NMR (75 MHz, dichloromethane-d_2, 25 °C) δ 133.2, 119.6, 90.6, 81.7, 78.7, 75.9; ^{13}C NMR (125 MHz, dichloromethane-d_2, −85 °C) δ 128, 119, 90.0. 80.9, 78.1, 75.5 (v br); high-resolution LSIMS calcd for $C_{23}H_{21}Ru_2$ M$^+$ − BF_4 500.9730, found 500.9716; UV (CD_2Cl_2) λ_{max} 384 (ϵ_{384} 9000), 468 (ϵ_{468} 9700) nm; UV ($CHCl_3$) λ_{max} 360, 450 nm; UV (THF) λ_{max} 329, 429 nm; UV (MeCN) λ_{max} 346, 431 nm; UV (MeOH) λ_{max} 335, 430 nm; UV (DMF) λ_{max} 339, 423 nm; UV (DMSO) λ_{max} 329, 427 nm; UV (PhCN) λ_{max} 349, 441 nm; IR (KBr) 3085, 2916, 1603 (s), 1498, 1449, 1404, 1205, 1076 (vs, br), 813, 698, 530 cm^{-1}; IR (CH_2Cl_2) 1603 (s), 1508, 1448, 1404, 1210, 1046 (vs, br), 837, 818 cm^{-1}; Raman (KBr) 1605 (s), 1449, 1144, 1103, 634 cm^{-1}. Anal. Calcd for $C_{23}H_{21}BF_4Ru_2$: C, 47.11; H, 3.60. Found: C, 46.98; H, 3.59; N, 0.17.

[Rc(CH)$_3$Rc]$^+$[PF$_6$]$^-$ (3b). Golden-brown plates of pure **3b** (106 mg, 0.16 mmol, 71%) were obtained from the corresponding crude alcohol (120 mg, 0.23 mmol) using the general method: IR (KBr) 3115, 2950, 1609 (s), 1503, 1449, 1409, 1210, 1136, 1036, 922, 837 (vs), 555 cm^{-1}; IR (CH_2Cl_2) 1598 (s), 848 (s); Raman (KBr) 1609 (s), 1449, 1374, 1305, 1283, 1251, 1209, 1140, 1103, 638 cm^{-1}; Raman (CH_2Cl_2) 1601 (s), 1449, 1280, 1210, 1144 cm^{-1}. Anal. Calcd for $C_{23}H_{21}PF_6Ru_2$: C, 42.86; H, 3.28. Found: C, 42.87; H, 3.31.

[Rc(CH)$_3$Rc]$^+$[BAr′$_4$]$^-$ (3c). Pure **3c** (80 mg, 0.059 mmol, 80%) was obtained from **3b** (53 mg, 0.080 mmol) and [Na]$^+$[BAr′$_4$]$^-$ (65 mg, 0.073 mmol) using the same method as for the preparation of **1c**: ^{1}H NMR (300 MHz, dichloromethane-d_2, 25 °C) δ 7.72 (br s, 8H), 7.56 (s, 4H), 7.29 (d, J = 13.5 Hz, 2H), 6.14 (t, J = 13.5 Hz, 1H), 5.44 (t, J = 1.8 Hz, 4H), 5.12 (t, J = 1.8 Hz, 4H), 4.80 (s, 10H); UV (Et_2O) λ_{max} 358, 442; UV (EtOAc) λ_{max} 358, 442; UV (1,4-dioxane) λ_{max} 376, 458; UV (benzene) λ_{max} 388, 479. IR (KBr) 1584 (s), 1357 (s), 1278 (vs), 1130 (vs, br), 901, 888, 839, 830, 713, 683, 669 cm^{-1}; IR (CH_2Cl_2) 1600 (s), 1355 (s), 1284 (vs), 1128 (vs, br), 898 (s), 672 cm^{-1}. Anal. Calcd for $C_{55}H_{33}BF_{24}Ru_2$: C, 48.47; H, 2.44. Found: C, 48.11; H, 2.93.

[Fc(CH)$_3$Fc″]$^+$[BF$_4$]$^-$ (4a). The general method was used to obtain dark platelets of **4a** (210 mg, 0.35 mmol, 59%) from crude FcCH═CHCH(OH)Fc″ (316, 0.59 mg): ^{1}H NMR (300 MHz, dichloromethane-d_2) δ 8.36 (d, J = 14.2 Hz, 1H), 7.83 (d, J = 13.1 Hz, 1H), 6.58 (dd, J = 14.2, 13.1 Hz, 1H), 5.01 (apparent t, J = ca.1.8 Hz, 2H), 4.86 (apparent t, J = 1.8 Hz, 2H), 4.37 (s, 5H), 3.68 (s, 1H), 1.99 (s, 6H), 1.67 (s, 6H), 1.49 (s, 6H), 1.48 (s, 6H); ^{13}C NMR (75 MHz, dichloromethane-d_2) δ 152.4 (CH), 145.5 (CH), 126.1 (CH), 104.1 (quat), 94.8 (quat), 91.7 (quat), 91.3 (quat), 83.5 (quat; remaining quat not observed), 80.2 (CH), 76.5 (CH), 72.0 (CH), 70.9 (CH), 10.7 (CH_3), 10.6 (CH_3), 9.0 (CH_3; remaining methyl resonance presumably overlapping); high-resolution LSIMS calcd for $C_{31}H_{37}Fe_2$ M$^+$ − BF_4 521.1594, found 521.1594; UV (CH_2Cl_2) λ_{max} 401 (ϵ_{401} 15 000), 438 (ϵ_{438} 14 000), 748 (ϵ_{748} 9100) nm; UV (THF) λ_{max} 413, 438, 747 nm; UV (MeCN) λ_{max} 395, 425, 723 nm; UV (DMSO) λ_{max} 397, 430, 722 nm; IR (KBr) 3095, 2956, 2906, 2856, 1553 (s), 1439, 1379, 1320, 1300, 1235, 1156, 1056 (s, br), 927, 902, 822, 694, 629 cm^{-1}; KBr (CH_2Cl_2) 2951, 2917, 1556 (s), 1382, 1236, 1083 (s), 1020 (s), 826 cm^{-1}. Anal. Calcd for $C_{31}H_{37}BF_4Fe_2$: C, 61.23; H, 6.13. Found: C, 60.83; H, 6.07.

[Fc(CH)$_3$Rc]$^+$[BF$_4$]$^-$ (5a). Brown microcrystals of **5a** (80 mg, 0.15 mmol, 52%) were obtained from the corresponding crude alcohol (150 mg, 0.29 mmol) by the general procedure: ^{1}H NMR (300 MHz, dichloromethane-d_2) δ 7.58 (d, J = 14.5 Hz, 1H), 7.41 (d, J = 12.2 Hz, 1H), 6.25 (dd, J = 14.5, 12.2 Hz, 1H), 5.91 (t, J = 1.9 Hz, 4H), 5.37 (t, J = 1.9 Hz, 4H), 5.05 (s, 5H), 4.86 (apparent s, 2H), 4.71 (apparent s, 2H), 4.27 (s, 5H); ^{13}C NMR (75 MHz, dichloromethane-d_2) δ 151.8, 124.4, 120.8, 95.0, 87.7, 86.0, 82.9, 79.4, 75.9, 72.6, 70.9; high-resolution LSIMS calcd for $C_{23}H_{21}FeRu$ M$^+$ − BF_4 455.0036, found 455.0053; UV (CH_2Cl_2) λ_{max} 404 (ϵ_{404} 11 000), 648 (ϵ_{648} 5000) nm; UV (THF) λ_{max} 373, 547 nm; UV (MeCN) λ_{max} 367, 553 nm. IR (KBr) 3095, 3025, 2916, 2846, 1598 (s), 1449, 1409, 1374, 1285, 1210, 1076 (vs), 922, 827, 693, 669 cm^{-1}; IR (CH_2Cl_2) 1596, 1075 cm^{-1}. Anal. Calcd for $C_{23}H_{21}BF_4FeRu$: C, 51.05; H, 3.91. Found: C, 50.92; H, 3.92; N, 0.14.

[Fc(CH)$_3$Rc]$^+$[PF$_6$]$^-$ (5b). Red-brown platelike crystals of **5b** (90 mg, 0.15 mmol, 60%) were obtained from crude FcCH═CHCH(OH)-Rc (140 mg, 0.25 mmol) by the general procedure: IR (KBr) 3115, 2926, 1598 (s), 1449, 1409, 1374, 1280, 1215, 1141, 1106, 833 (s), 698, 634, 555 cm^{-1}; IR (CH_2Cl_2) 1599, 840 cm^{-1}. Anal. Calcd for $C_{23}H_{21}PF_6FeRu$: C, 46.09; H, 3.53. Found: C, 46.33; H, 3.50; N, 0.13.

X-ray Crystallography. Crystals of **1b**, **2b**, **3b**, **4a**, and **5b** were grown by layering dichloromethane solutions with diethyl ether, while **3c** crystals were grown by layering a THF solution with pentane. Crystallographic data were acquired using Mo Kα radiation (λ = 0.710 69 Å) using Enraf-Nonius CAD-4 or Kappa CCD diffractometers (CCD intensity data were processed using the programs DENZO and SCALEPACK[67]). Solution and refinement was carried out using

(65) Brookhart, M.; Grant, B.; Volpe, A. F. *Organometallics* **1992**, *11*, 3920−3922.

(66) Chávez, I.; Alvarez-Carena, A.; Molins, E.; Roig, A.; Maniukiewicz, W.; Aranacibia, A.; Aranacibia, V.; Brand, H.; Manríquez, J. M. *J. Organomet. Chem.* **2000**, *601*, 126−132.

(67) Otwinowski, Z.; Minor, W. In *Processing of X-ray Diffraction Data Collected in Oscillation Mode, Methods Enzymol.*; Carter, C. W., Sweet, R. M., Eds.; Academic Press: New York, 1997; Vol. 276.

Table 4. Details of Crystal Structure Determinations

	1b	2b	3b	3c	4a	5b
formula	$C_{23}H_{21}F_6Fe_2P$	$C_{39}H_{53}F_6Fe_2P$	$C_{23}H_{21}F_6PRu_2$	$C_{55}H_{33}BF_{24}Ru_2$	$C_{31}H_{37}BF_4Fe_2$	$C_{23}H_{21}F_6FePRu$
formula wt	554.07	778.48	644.51	1362.76	608.13	599.29
cryst appearance	red fragment	green blade	dark golden plate	dark red block	greenish fragment	dark brown plate
cryst size/mm^3	0.44 × 0.37 × 0.30	0.41 × 0.19 × 0.15	0.39 × 0.39 × 0.09	0.2 × 0.2 × 0.2	not measured	0.39 × 0.37 × 0.09
cryst system	orthorhombic	orthorhombic	monoclinic	monoclinic	monoclinic	monoclinic
space group	*Pbcn*	$P2_12_12_1$	*C*2/*c*	$P2_1/c$	$P2_1/n$	*C*2/*c*
diffractometer	CAD-4	CAD-4	CAD-4	Kappa CCD	CAD-4	CAD-4
T/K	85	85	85	150	85	85
a/Å	14.420(3)	9.446(3)	26.409(6)	16.5037(6)	8.702(3)	26.411(6)
b/Å	12.267(2)	17.746(5)	15.004(3)	18.7047(3)	20.419(4)	14.753(3)
c/Å	24.062(5)	21.634(7)	11.970(3)	18.3623(5)	15.446(3)	11.900(3)
β/deg	90	90	113.83(2)	111.946(2)	93.24(2)	112.92(2)
V/Å^3	4256.3(14)	3626.5(19)	4338.6(17)	5257.6(3)	2740(12)	4270.7(17)
Z	8	4	8	4	4	8
D_{calc}/g cm^{-3}	1.729	1.426	1.973	1.722	1.474	1.864
μ/mm^{-1}	1.499	0.902	1.526	0.698	1.103	1.522
F(000)	2240	1632	2528	2688	1264	2384
θ_{max}	25.0	25.0	25.0	27.5	25.0	25.0
no. of reflctns	9150	11 341	10 256	40 156	11 091	10 102
indep^t reflctns	3752	6354	3818	11 887	4830	3753
R_{int}	0.034	0.019	0.0144	0.0568	0.026	0.0172
absorp^n corrctn	none	none	ψ scan	from equiv refs	ψ scan	ψ scan
soln method	SHELXS-97	SHELXS-97	SHELXS-97	SHELXS-97	SHELXS-86	isomorph. with **3b**
refinmnt program	SHELXL-97	SHELXL-97	SHELXL-97	SHELXL-97	CRYM programs	SHELXL-97
refinmnt method	full matrix F^2	full matrix F^2	full matrix F^2	full matrix F^2	full matrix F^2	full matrix F^2
data/restr/ param	3752/0/310	6354/0/645	3818/0/392	11887/60/736	4830/0/343	3753/0/382
R1, wR2 (all data)	0.101, 0.133	0.034, 0.060	0.024, 0.049	0.1269, 0.1817	0.059, 0.113	0.040, 0.076
final GOF (on F^2)	2.66	1.51	1.76	1.021	2.73	2.32
$\Delta\rho_{max}$, $\Delta\rho_{min}$/e Å^{-3}	1.50, −0.59	0.37, −0.38	0.46, −0.45	1.24, −1.24	1.21, −0.80	1.21, −0.89

SHELXS[68] or CRYM[69] programs (as specified in Table 4). Details of the crystal data, data collection, and structure solutions and refinements are given in Table 4; additional details available as Supporting Information in the case of **2b**, **3c**, **4a**, and **5b**, while the Supporting Information for ref 28 gives full details for the structures of **1b** and **3b**. The two largest difference peaks in the refined structure of **1b** indicate disorder, whereby the cations can adopt two alternative orientations that are related to one another by an approximate reflection in a plane perpendicular to the plane of the allylium bridge and passing through both Fe atoms. This type of disorder was previously seen in a number of other polymethine structures, for example, in that of $[Me_2N(CH)_7NMe_2]^+[Cl]^-\cdot 4H_2O$.[70] However, in our case, one of the orientations is clearly much less important than the other (∼1:9); we were not able to adequately model the disorder, and so no disorder is included in the resulting structure. However, a number of anomalous bond lengths and angles in the structure reflect the presence of unmodeled disorder. In the structure of **3c**, two of the largest difference peaks possibly relate to an alternative orientation of the allylium bridge similar to that in **1b**; again the disorder was not modeled, but here there are no unusual bond lengths arising from the unmodeled disorder. Some of the CF_3 groups of the anion in **3c** were modeled, using restraints, as rotationally disordered. In the structures of both **3b** and **5b**, the hexafluophosphate anions occupy two different Wyckoff sites; at both sites there is orientational disorder, which was successfully modeled as two distinct orientations on each site. For each site, the ratios between the two orientations are slightly different in the two structures. Difference maps, as well as the final goodness of fit, for the structure of **4a** indicate some disorder associated with the tetrafluoroborate anion; however, we could not develop a chemically reasonable model for this disorder and, therefore, treated it as an ordered group in the refinement. Further details of the structures are given in the Supporting information.

Acknowledgment. Support from the National Science Foundation, Air Force Office of Scientific Research (AFOSR) at Caltech is gratefully acknowledged. The research described in this paper was performed in part by the Jet Propulsion Laboratory (JPL), California Institute of Technology, as part of its Center for Space Microelectronics Technology and was supported by the Ballistic Missile Defense Initiative Organization, Innovative Science and Technology Office through an agreement with the National Aeronautics and Space Administration (NASA). We thank Kenneth Calgren for his assistance with Raman measurements, Dr. Paul Roussel for his assistance with low-temperature NMR experiments, Dr. Andrew Cowley for his efforts with a highly disordered crystal of **3c**·*x*CH_2Cl_2, and Johnson Matthey for a loan of ruthenium precursors. We also thank the reviewers of the manuscript for helpful comments.

Supporting Information Available: Details of the crystal structure determinations of **2b**, **3c**, **4a**, and **5b** in CIF format (details for the structures of **1b** and **3b** have previously appeared as Supporting Information for ref 28). Figure showing cyclic voltammograms for **2a**; ^{1}H and ^{13}C NMR spectra for McCH═CHBr {Mc = Fc, Fc″, Rc} (PDF). This material is available free of charge via the Internet at http://pubs.acs.org.

JA012472Z

(68) Sheldrick, G. M. *SHELXS-86, SHELXS-97,* and *SHELXL-97, Programs for Crystallography*; University of Göttingen: Göttingen, Germany, 1986 and 1997.
(69) Duchamp, D. J. Am. Crystallogr. Assoc. Meet., Bozeman, MT, 1964; Paper B14.
(70) Groth, P. *Acta Chem. Scand.* **1987**, *B41*, 547−550.